**ERNEST ORLANDO LAWRENCE
BERKELEY NATIONAL LABORATORY**

Understanding Loss Mechanisms and Efficiency Improvement Options for HCCI Engines Using Detailed Exergy Analysis

Samveg Saxena[1], Iván Dario Bedoya[2], Nihar Shah[1], Amol Phadke[1]

[1] Environmental Energy Technologies Division
    International Energy Studies Group

[2] University of Antioquia

June 20, 2012

Disclaimer

While this document is believed to contain correct information, neither the United States Government nor any agencies thereof, The Regents of the University of California, nor any of their employees, makes any warranty, express or implied, or assumes any legal responsibility for the accuracy, completeness, or usefulness of any information, apparatus, product, or process disclosed, or represents that its use would not infringe privately owned rights. Reference herein to any specific commercial product, process, or service by its trade name, trademark, manufacturer, or otherwise, does not necessarily constitute or imply its endorsement, recommendation, or favoring by the United States Government or any agency thereof, or The Regents of the University of California. The views and opinions of authors expressed herein do not necessarily state or reflect those of the United States Government or any agency thereof, or The Regents of the University of California.

Ernest Orlando Lawrence Berkeley National Laboratory is an equal opportunity employer.

1   Contents

List of Figures

List of Tables

Abbreviations and Acronyms

ϕ Fuel-air equivalence ratio

CA_x Crank angle timing of x% of the total heat release, i.e. CA50 is the crank angle timing for 50% heat release

CFD   Computational fluid dynamics

CO   Carbon monoxide

EGR   Exhaust gas recirculation

FID   Flame ionization detector

HC   Hydrocarbons

HCCI   Homogeneous Charge Compression Ignition

$IMEP_g$ Gross indicated mean effective pressure

P_{BDC} In-cylinder pressure at bottom dead center

P_{man} Intake manifold pressure

RPM   Revolutions per minute

TDC   Top dead center

Executive Summary

This report presents a detailed exergy analysis of homogeneous charge compression ignition (HCCI) engines, including a crank-angle resolved breakdown of mixture exergy and exergy destruction. Exergy analysis is applied to a multi-zone HCCI simulation including detailed chemical kinetics. The HCCI simulation is validated against engine experiments for ethanol-fueled operation. The exergy analysis quantifies the relative importance of different loss mechanisms within HCCI engines over a range of engine operating conditions. Specifically, four loss mechanisms are studied for their relative impact on exergy losses, including 1) the irreversible combustion process (16.4-21.5%), 2) physical exergy lost to exhaust gases (12.0-18.7%), 3) heat losses (3.9-17.1%), and 4) chemical exergy lost to incomplete combustion (4.7-37.8%). The trends in each loss mechanism are studied in relation to changes in intake pressure, equivalence ratio, and engine speed as these parameters are directly used to vary engine power output. This exergy analysis methodology is proposed as a tool to inform research and design processes for energy storage, transport and conversion technologies, particularly by identifying the relative importance of each loss mechanism in determining system efficiency.

Objective and Scope

This study applies exergy analysis to a multi-zone HCCI engine model which captures detailed chemical kinetics with the following objectives:

1. Quantify exergy loss mechanisms in HCCI engines through detailed chemical kinetic engine cycle simulations.

2. Explore how the loss mechanisms change when different engine operating conditions are used, particularly by changing operating parameters that govern power output for an HCCI engine (intake pressure, equivalence ratio and engine speed in this paper).

3. Develop HCCI engine exergy analysis to provide information that is useful in prioritizing HCCI engine research directions.

1   Introduction

1.1   HCCI Engines

HCCI engines combine characteristics of both spark-ignited engines and diesel engines. Similar to spark-ignited engines, HCCI uses a pre-mixed fuel-in-air charge, and similar to diesel engines, the mixture is compression ignited. The diluted premixed charge facilitates a relatively uniform autoignition event rather than a non-premixed flame found in diesel engines, and thus HCCI engines can achieve fewer emissions of particulate matter. The diluted mixtures characteristic of HCCI engines cause lower post combustion temperatures resulting in significantly reduced emissions of nitrogen oxides (NO_x). Significant improvements in efficiency can be gained in HCCI engines as compared with spark-ignited because of the elimination of the intake throttle, and the relatively high compression ratios that are required in achieving autoignition.

1.2   Exergy Analysis

Exergy is a thermodynamic property that is used to measure the theoretical maximum useful work that a system can produce, and exergy analysis can be used in understanding a) the relative contribution of different loss mechanisms that result in performance below the maximum work output, and b) the theoretical maximum work output. Exergy analysis is applied to an ethanol fueled HCCI engine in this study to provide an understanding of the fraction of overall exergy efficiency that is lost to four different loss mechanisms. A procedure for coupling exergy analysis with engine simulations is developed which enables visualization of exergy losses on a crank-angle resolved basis, and then this procedure is used across a wide range of engine operating conditions to provide an understanding of how the different loss mechanisms change with varying engine operating parameters. The change in the contribution from each loss mechanism over different engine operating points dictates the maximum exergy efficiency operating points. This information can then be used throughout the engine research and design process, for instance: 1) to guide investment decisions that weigh which research efforts will produce the greatest efficiency gains, i.e. which loss mechanisms are the most worthwhile to address from an efficiency standpoint, and 2) by overlaying the loss mechanisms with engine operating and design constraints (like excessive ringing), exergy analysis can be used in the engine mapping process to provide a picture of where and why local maxima in efficiency will occur.

Exergy analysis has been applied to spark ignited and diesel engines in several prior studies [1-3] to explore the interaction of loss mechanisms with different engine design and operating parameters. In an HCCI context, exergy analysis has been applied in prior studies [3-5] as well, however many of these prior studies significantly simplify the in-cylinder processes and approximate them as ideal thermodynamic cycles. This simplification ignores the complex dynamics that govern combustion timing in HCCI engines, and thus the present study uses detailed chemical kinetics in HCCI engine simulations to provide a more accurate account of the loss mechanisms and how they are influenced by different engine operating parameters. One study [6] used a more detailed single-zone model with detailed chemical kinetics to perform exergy analysis of a dual-fueled (natural gas and n-heptane) HCCI engine. Although this study [6] used similar analysis techniques to the present study, the focus was on the influence of varying fuel composition (natural gas and n-heptane fractions) and EGR fractions. Nine operating conditions were simulated, however a detailed breakdown of loss mechanisms was not given. The present study provides a more thorough understanding of losses in an HCCI engine by exploring 252 operating points that focus on high power output conditions, while also providing a detailed breakdown of the loss mechanisms and how they change with varying operating conditions.

2 Description of Numerical Methodology and Validation with Experimental Results

2.1 HCCI Engine Modeling Methodology

The HCCI simulations are run using a multi-zone model [7], where each zone is treated as a homogeneous reactor. Mass interactions between zones are not considered, while heat transfer to the walls is modeled with the Woschni correlation [8,9], and an external heat transfer area fraction for each zone. Core zones are assigned a small heat transfer area fraction, while boundary zones are given a larger heat transfer area fraction[1]. Only the closed portion of the cycle is considered. A chemical kinetic mechanism, updated in 2004, for Ethanol is used from Lawrence Livermore National Laboratory [10]. The model was used to simulate engine conditions representing the HCCI experimental setup used in previous studies by the authors [11-14].

2.2 Validation of Model Results Against Experiments

The HCCI simulation methodology described in section 2.1 provides a good estimate of in-cylinder variables such as the combustion timing, peak pressure, $IMEP_g$, indicated efficiency, and NO_x emissions; however, it tends to overpredict the maximum pressure rise rate and underpredict HC and CO emissions compared with experimental engine measurements [14]. Greater accuracy of pressure rise rates and HC emissions can be obtained using a larger number of zones (40 and above) along with simulation methods that define zone average temperature and mass fraction for each zone using CFD analysis prior to the multi-zone chemical kinetic simulations[2]. The accurate prediction of CO emissions requires even further computational burden by taking mass transfer between zones into account [7,15,16,17]. These more advanced simulation methods are more computationally expensive and make it difficult to run the large number of simulation conditions that were explored in this study (252 operating points in total) while not adding significantly more insight for the purposes of exergy analysis.

Figure 1 through Figure 5 compare simulated results against experimental measurements. Although the simulated and experimental results are not in perfect agreement, these plots and their associated discussions are presented to convey that the model and experiments are in general agreement and to help the reader understand the magnitude and cause of any discrepancies.

Figure 1 shows a comparison of experimental and simulated in-cylinder pressure for two different intake manifold pressures, each at three different combustion timings, to demonstrate that the 10-zone HCCI model is capable of generating accurate results, despite the known over predictions in maximum pressure rise rate.

---

[1] A table of mass fraction and external heat transfer area fraction for each zone is presented in the Appendix.

[2] A parametric study of the influence of number of simulated zones upon exergy analysis results is presented in the Appendix. The results show that the number of simulated zones do not significantly impact the exergy analysis results, thus 10 zones are used throughout the paper.
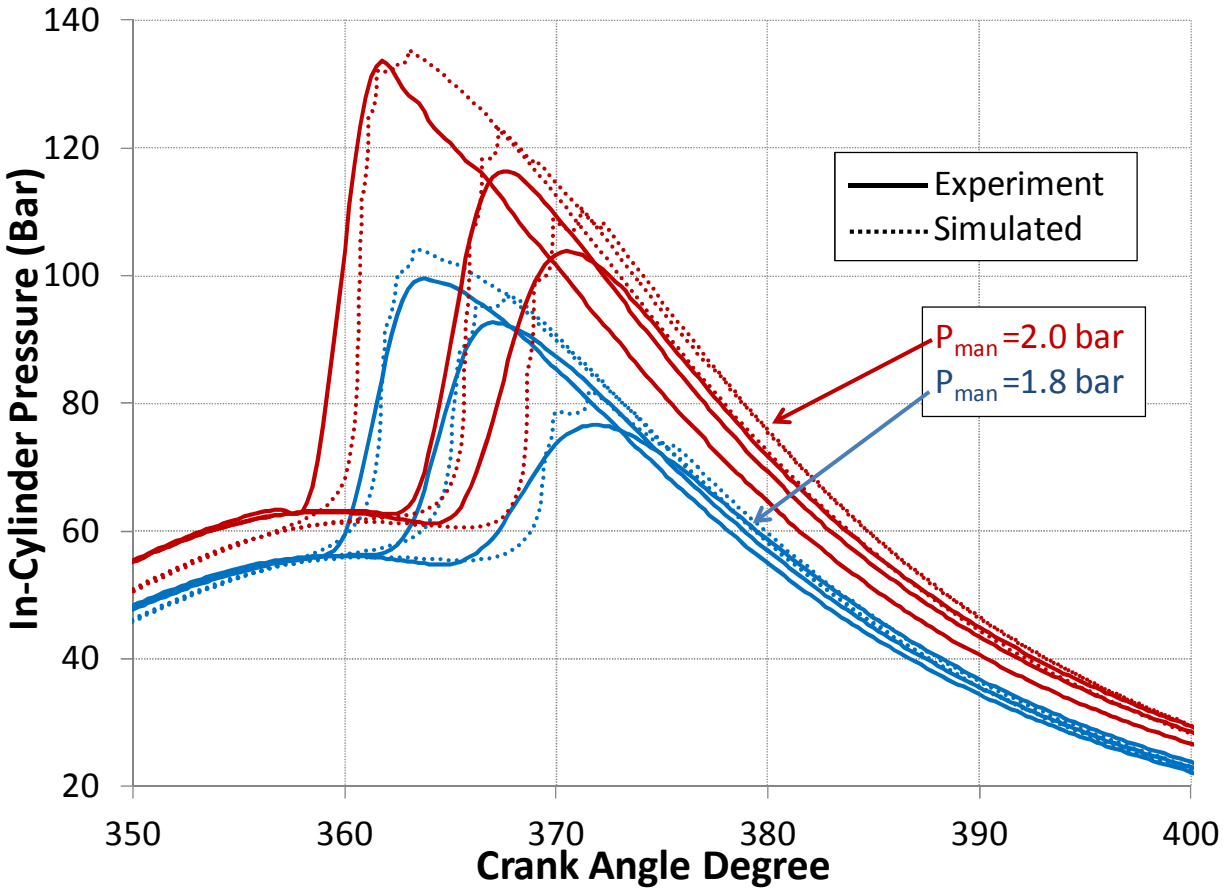
Figure 1 - Comparison of experimental and simulated in-cylinder pressure traces

Figure 2 through Figure 5 compare data that is calculated through post-processing of simulated and experimental data. In each plot, a wide range of combustion timings are plotted for two different intake pressures and two different equivalence ratios. Lines of best fit are presented for each data set, with experimental fits displayed as a solid lines and simulated fits as dashed lines. Experimental data points are plotted as the average from 300 consecutive engine cycles, and the error bars for each point represent one standard deviation among 300 cycles of data.

Figure 2 shows the power output, calculated as gross indicated mean effective pressure, for several engine operating points. In all cases plotted, the power output results agree at a combustion timing of 6 CAD ATDC, however the model tends to overpredict power output at early combustion timings and underpredict power output at late combustion timings. It is important to note that the experimental data was collected on a 4-cylinder engine with only one cylinder firing. As a result, the engine block temperature was colder than normal engine operation and thus the heat losses for the experimental cases may be artificially high, thereby causing lower power output – particularly for early combustion timings which allow more time for heat loss. Experimental data was not collected for late combustion timings because it was difficult to maintain stable combustion long enough to collect a complete data set, thus the downward slope for experimental data at late combustion timings is not apparent.

Figure 2 - Comparison of gross indicated power output for experimental and simulated cases for several intake pressures, equivalence ratios and combustion timings. 1800 RPM, ethanol fueled

Figure 3 compares the combustion efficiency for several simulated and experimental engine operating points. The modeled and experimental combustion efficiencies agree at early combustion timings, while the model tends to underpredict combustion efficiency at later combustion timings. One important consideration is that the experimental combustion efficiencies are calculated from CO and unburned HC emissions, however it is assumed that all HCs are unburned ethanol. The simulations, however, give more specific information about the types of HCs, thereby allowing a more detailed calculation of combustion efficiency using the enthalpies of specific exhaust hydrocarbon components. Additionally, it is important to note that experimental exhaust hydrocarbon measurements are taken using a flame ionization detector (FID) which introduces some uncertainty when measuring unburned alcohol exhaust components. FIDs are known to have a response factor of between 1.5-1.7 for ethanol [18], meaning that an FID detects between 1.5-1.7 carbon atoms when there are actually two carbon atoms in ethanol.
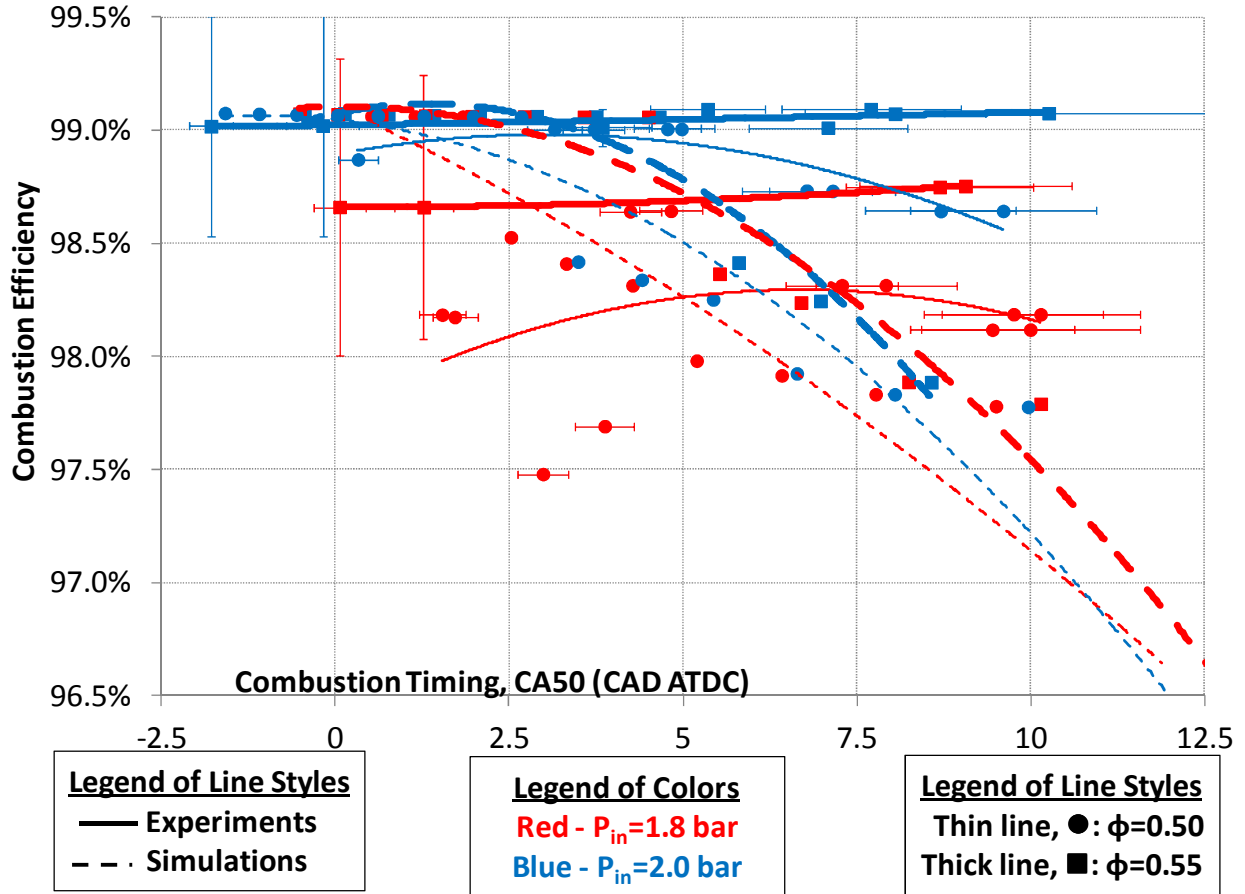
Figure 3 - Comparison of combustion efficiency for experimental and simulated cases for several intake pressures, equivalence ratios, and combustion timings. 1800 RPM, ethanol fueled

Figure 4 shows the unburned CO emissions for several experimental and simulated engine operating points. As expected for the 10-zone model approach, CO emissions are underpredicted with the model. More accurate predictions of CO emissions can be generated using more complex modeling techniques, which couple CFD and chemical kinetics to model the mass transfer between zones, however as mentioned above, this would cause computation times to be too large for the 252 operating points that are explored in this study.
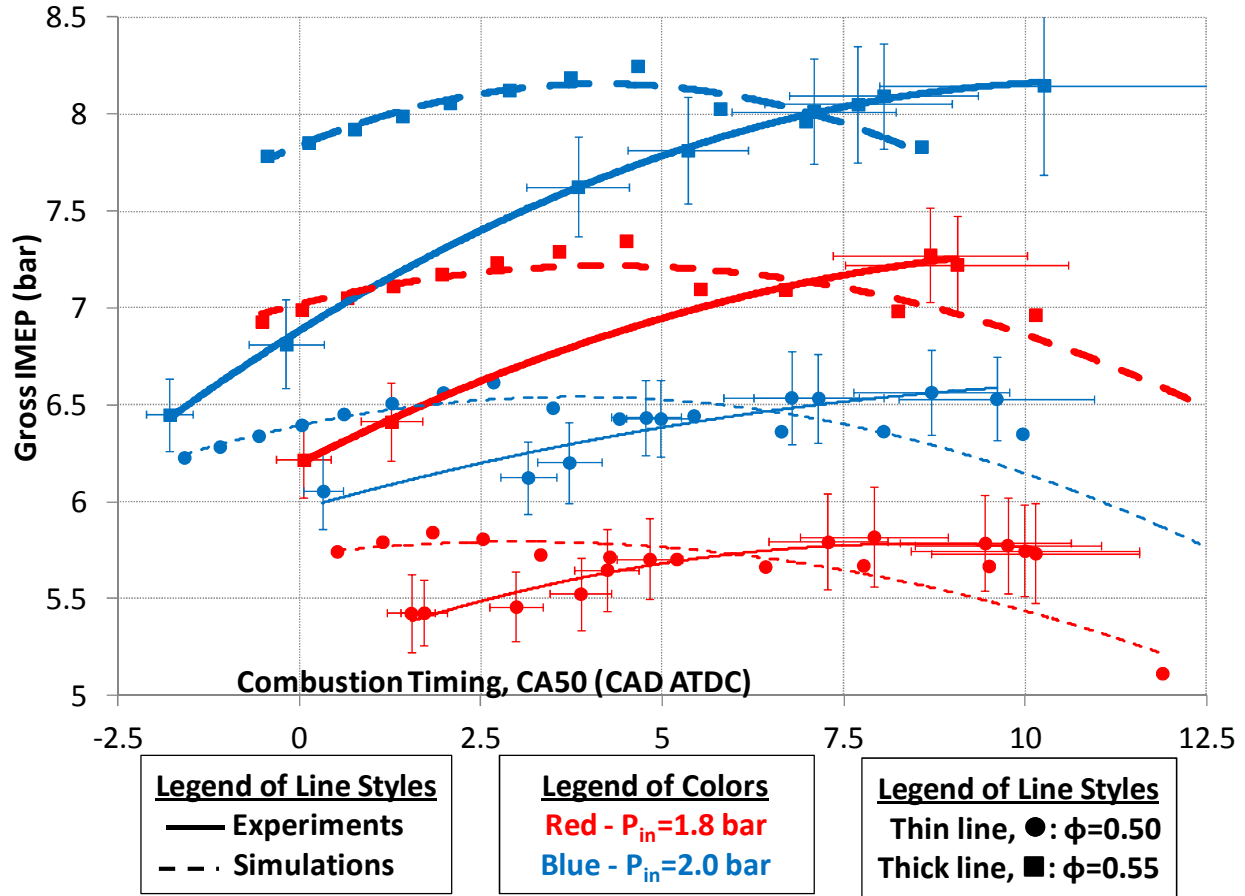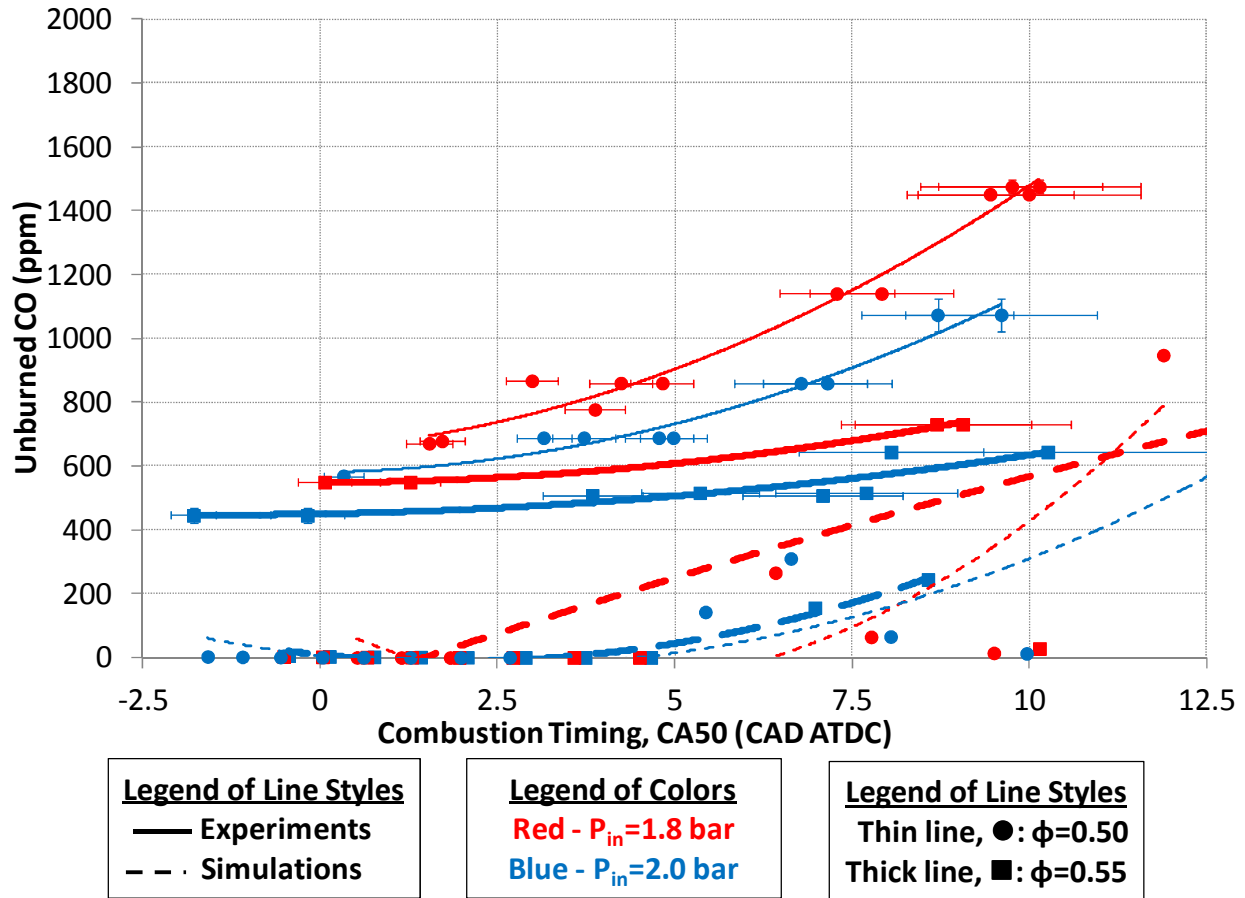
Figure 4 - Comparison of carbon monoxide emissions for experimental and simulated cases for several intake pressures, equivalence ratios, and combustion timings. 1800 RPM, ethanol fueled

Figure 5 shows the exhaust temperature for experimental operating conditions, and the in-cylinder EVO temperature for simulated operating conditions. It is difficult to directly compare the two quantities because the simulated EVO temperatures do not account for temperature decreases from heat loss and expansion that would occur as the burned gases leave the cylinder and proceed to where exhaust gas temperature is measured in the experiments. It is, however, still useful to note that the equivalence ratio and pressure dependence of the EVO and exhaust temperatures agree.
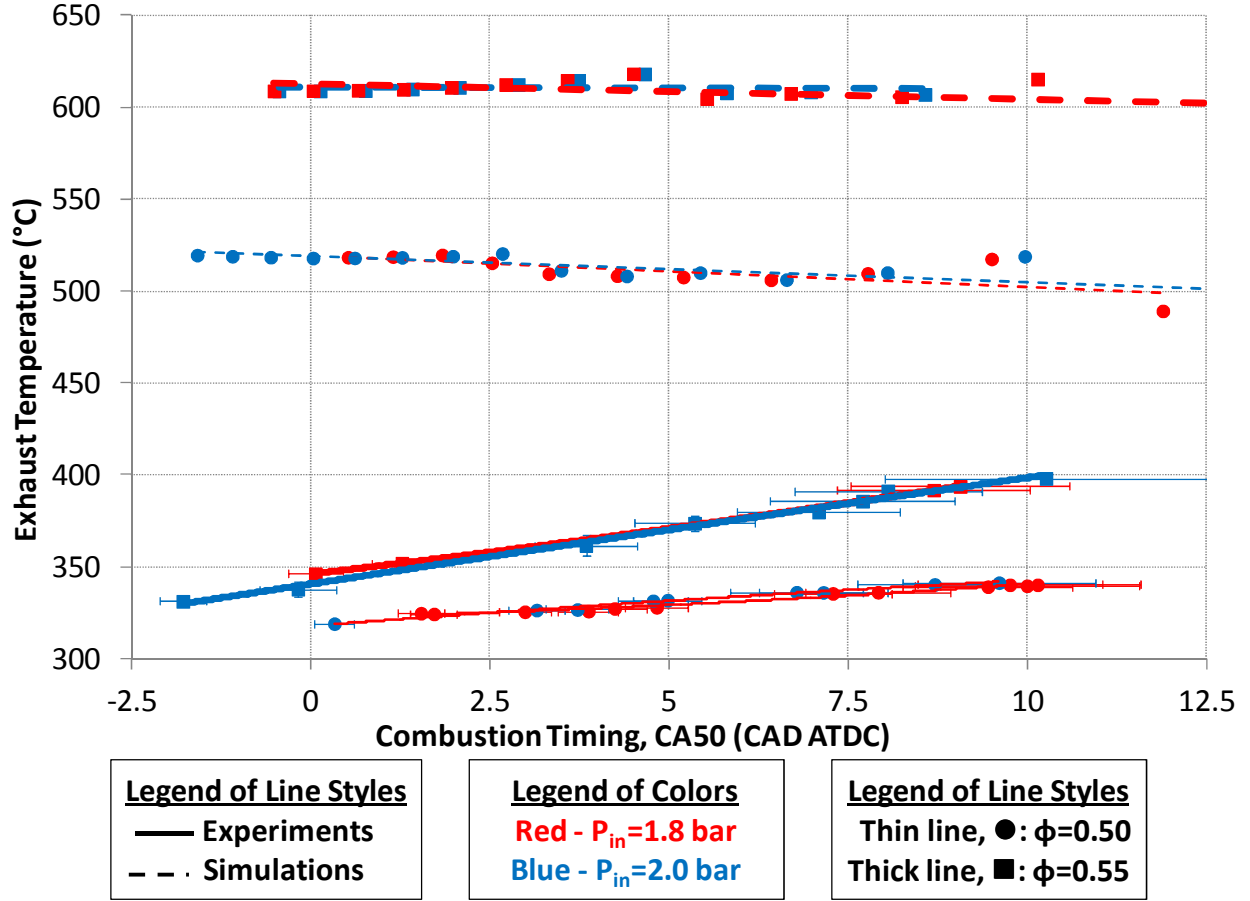
Figure 5 - Comparison of exhaust (experimental) and EVO (simulated) temperatures for several intake pressures, equivalence ratios, and combustion timings. 1800 RPM, ethanol fueled

In the results section of this paper several exergy loss mechanisms are discussed, including exergy losses from combustion, heat loss, unburned species, and exhaust. By comparing experimental and simulated data in Figure 1 through Figure 5, the authors aim to give the reader awareness of some differences between the experimental and simulated results to develop an understanding of how simulated exergy destruction mechanisms may differ from actual engine conditions. Broadly speaking, the simulated and experimental comparisons suggest that exergy losses to unburned species may be underpredicted in the simulations because of lower simulated CO emissions, and exergy losses to heat loss may be underpredicted (although heat losses in the experiments are artificially high because of single-cylinder operation).

2.3   Crank-Angle Resolved Exergy Analysis

The 10-zone model results are post-processed taking into account only species that are present with mole fractions above 0.01% at any time during the closed cycle simulations. Enthalpy and entropy of the mixture are calculated using NASA polynomials with coefficients for each species specified in the thermodynamics property file of the ethanol mechanism [10].

Total exergy of the in-cylinder mixture is calculated using Eq. 1 [1]:

$$a_{total} = (u - u_0) + P_0(v - v_0) - T_0(s - s_0)$$ (Eq. 1)

In Eq. 1, u, v, and s are the specific internal energy, specific volume, and specific entropy. All quantities with

a subscript 0 are the respective properties for the dead state defined in Table 1:

Temperature, T_0		298.15 K
Pressure, P_0		1.01325 bar
Composition (mole fractions)	N_2	0.7565
	O_2	0.2029
	H_2O	0.0313
	Ar	0.0090
	CO_2	0.0003

Table 1 - Properties of the dead state

The physical and chemical components of exergy are calculated with Eq. 2 and Eq. 3 respectively [19]:

$$a_{phys} = (u - u_*) + P_0(v - v_*) - T_0(s - s_*) \tag{Eq. 2}$$

$$a_{chem} = \mu_* - \mu_0 \tag{Eq. 3}$$

In Eq. 2 and 3, subscript * represents the restricted dead state for the in-cylinder mixture, which is defined as the in-cylinder mixture taken to the dead state temperature and pressure (T_0 and P_0), but not necessarily having the dead state composition. In Eq.3, μ_* and μ_0 are the chemical potential for the restricted dead state and the actual dead state, calculated with Eq. 4:

$$\mu = h - T_0 s \tag{Eq. 4}$$

Exergy destruction from the combustion process is calculated using the Gouy-Stodola law, Eq. 5, applied between the times when heat release from combustion starts and ends (i.e. from CA0.005 and CA0.995):

$$x_{dest,combustion} = T_0 s_{gen} \tag{Eq. 5}$$

Exergy loss from heat loss is calculated using Eq. 6 [19,20], where the heat losses (Q_{out}) are calculated using the Woschni heat transfer coefficient [8] (within the 10-zone HCCI model). In this analysis, the term T in eqn. 6 is the mass averaged in-cylinder temperature:

$$x_{HL} = Q_{out}\left[\frac{T - T_{walls}}{T \cdot T_{walls}}\right]T_0 \tag{Eq. 6}$$

Overall exergy efficiency is calculated using Eq. 7, where the numerator represents the total indicated work against the surroundings, and the denominator is the total exergy in the fuel.

$$\eta_{ex} = \frac{\sum_{\theta=180°}^{540°}(P - P_0)dV}{a_{fuel} \cdot m_{fuel}} \tag{Eq. 7}$$

The fuel exergy, a_{fuel}, is calculated using Eq. 8 with Gibb's free energies, g [1]:

$$a_{fuel} = -g_{rxn} = -\left(g_{products} - g_{reactants}\right) \tag{Eq. 8}$$

Eq. 8 is applied assuming complete combustion for ethanol fuel at the simulated equivalence ratios (i.e. the only products are CO_2, H_2O, O_2 and N_2).

In the results section of this paper, two further quantities are reported, 1) the physical exergy lost to exhaust

gases, and 2) the inaccessible chemical exergy due to incomplete combustion. The first quantity is determined by simply using the physical exergy (Eq. 2) at exhaust valve open timing. The second quantity is determined as the difference between the Gibb's free energy of the actual reaction occurring in the engine simulations and the fuel exergy calculated in Eq. 8.

2.4   Simulated Engine Conditions

One objective of this study is to understand how exergy loss mechanisms change as operating parameters are changed to vary engine power output. Specifically, changes in three operating parameters are explored, 1) intake pressure, 2) equivalence ratio, and 3) engine speed. For each of the three parameter sweeps, 12 combustion timings are simulated with combustion occurring from slightly before TDC to the point where misfire occurs. Combustion timing is adjusted by changing the intake temperature. Table 2 shows the input parameters that were used to define the engine for this study, and Table 3 shows the operating points that were explored.

Compression ratio	16.15	
Displacement volume	475 cc	
Bore diameter	79.55 cm	
Connecting rod/crank radius	3.0157	
Woschni Heat transfer coefficients	a	0.035
	b	0.80
	c	0.00
Number of zones	10	

Table 2 - Input parameters to specify engine in simulations

Sweep name	P_{BDC} (bar abs)		ϕ		Engine speed (RPM)		CA50
Intake Pressure	1 1.6 1.2 1.8 1.4 2.0		0.40		1800		~TDC to Misfire
Equivalence ratio #1	1.0		0.25 0.40 0.30 0.45 0.35		1800		~TDC to Misfire
Equivalence ratio #2	1.8		0.25 0.40 0.30 0.45 0.35		1800		~TDC to Misfire
Engine speed	1.8		0.40		1000 1600 1200 1800 1400 2000		~TDC to Misfire

Table 3 - Operating conditions explored for exergy analysis

3   Results

In this section, sample results from the crank-angle resolved exergy analysis methodology (discussed in section 2.3) are first reviewed. The insights provided by the crank-angle resolved methodology are then applied over the entire range of operating conditions listed in Table 3 to show the relative impact of several exergy loss mechanisms and how these loss mechanisms change over different engine operating conditions. Finally, the applicability of these results for engine research and design are discussed.

3.1   Crank-Angle Resolved Exergy Analysis

The exergy analysis methodology discussed in section 2.3 is used to compute crank-angle resolved exergy quantities to provide insight into the causes of exergy loss. Figure 6 and Figure 7 show a sample of the results from crank-angle resolved exergy analysis for a single operating point. In Figure 6, the total exergy, physical exergy and chemical exergy are overlaid with the in-cylinder pressure. Total exergy represents the maximum theoretical work that can be extracted from the in-cylinder gases if they are brought to physical and chemical equilibrium with the environment. Given that an engine directly extracts physical exergy through piston expansion, it is useful to separate the total exergy into physical and chemical components as seen in Figure 6.
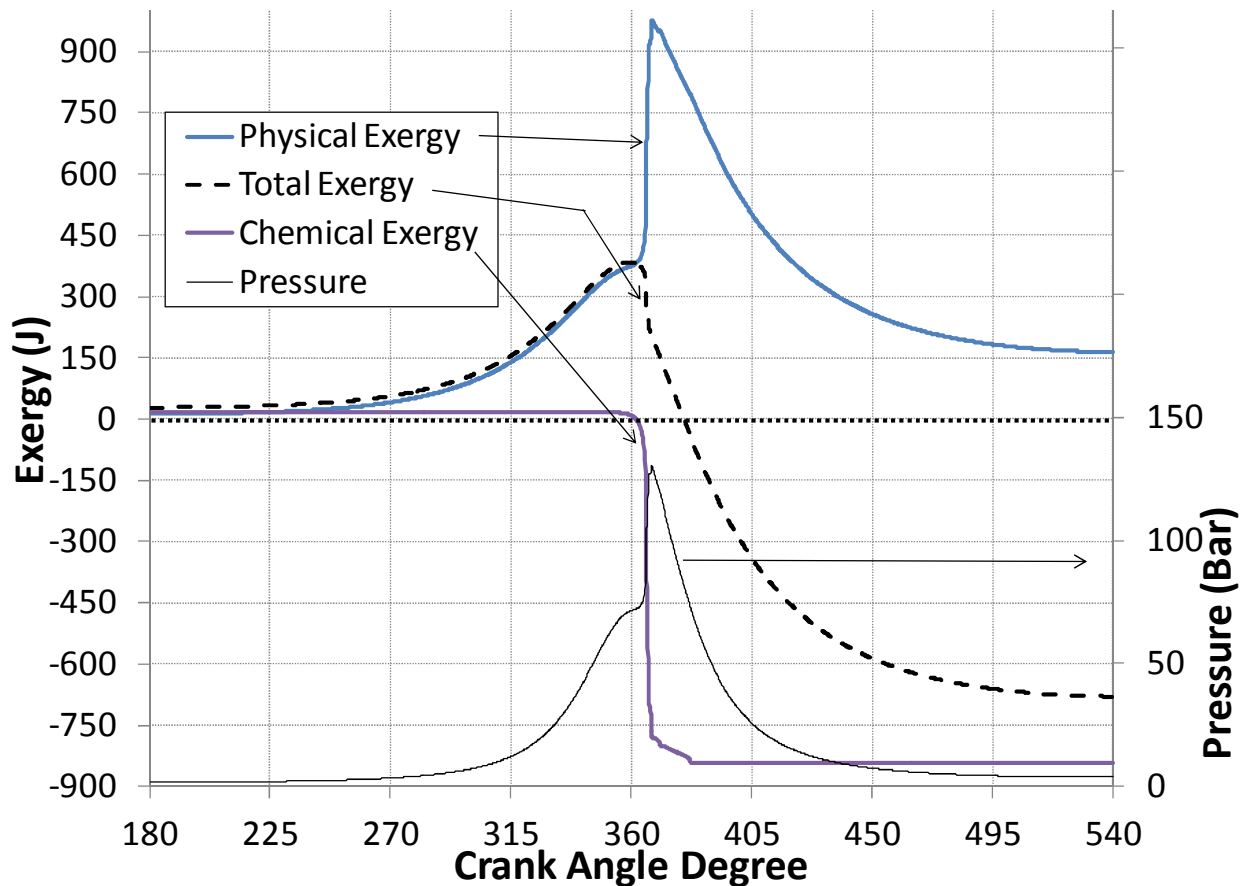
Figure 6 - Crank-angle resolved exergy (total, physical and chemical) for a single operating point with P_{BDC}=1.8 bar, ϕ=0.40, 1800 RPM, Ethanol fuel

By separating the physical and chemical components of exergy of the in-cylinder gas mixture, as in Figure 6, it is easy to see the amount of unused exergy that is lost to exhaust gases. Additionally, it can be seen in Figure 6 that the change in chemical exergy during the combustion process is larger than the change in

10

physical exergy, and this difference is largely caused by the irreversibilities that occur during combustion. Figure 7 shows a crank-angle resolved plot of exergy destruction, including the losses from the combustion process.
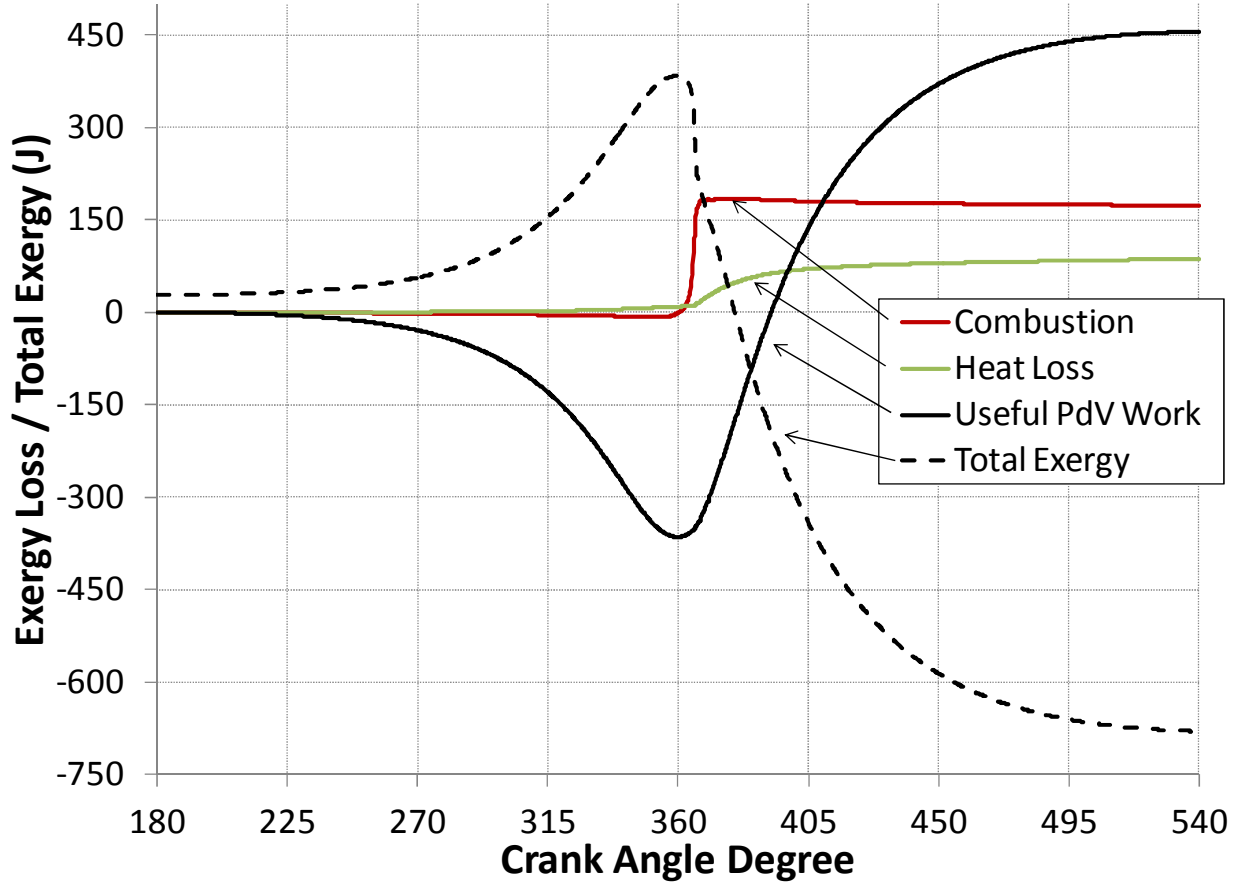
Figure 7 - Crank-angle resolved cumulative exergy destruction for a single operating point with P_{BDC}=1.8 bar, ϕ=0.40, 1800 RPM, Ethanol fuel

Figure 7 shows the cumulative exergy destruction from irreversible combustion, heat loss, and also the exergy added or subtracted from the in-cylinder gases due to the compression and expansion processes (PdV Work). In Figure 7, negative values represent exergy added to the in-cylinder gases and positive values represent exergy removed from the in-cylinder gases (through exergy destruction or exergy transfer out of the system). For the results in Figure 6 and Figure 7 (and their equivalent plots for all other operating conditions), the following exergy balance holds true:

$$A_{total}\left(\theta\right) = A_{phys}\left(\theta\right) + A_{chem}\left(\theta\right)$$

$$A_{total}\left(\theta\right) = A_{total}\left(\theta = 180^{\circ}\right) - \left[A_{dest,comb}\left(\theta\right) + A_{HL}\left(\theta\right) - A_{work}\left(\theta\right)\right]$$

where A_{total} is the total exergy, A_{phys} and A_{chem} are the physical and chemical components of total exergy, $A_{dest,comb}$ is the exergy destroyed from irreversible combustion, A_{HL} is the exergy loss from heat loss, and A_{work} is the exergy loss from useful work (i.e. the compression and expansion processes).

The crank-angle resolved exergy analysis demonstrated in Figure 6 and Figure 7 provide insight into the timing and relative quantity of different loss mechanisms. The physical exergy plotted in Figure 6 can be used to quantify the amount of unused exergy that is lost to exhaust gases at exhaust valve open. Additionally, by

11

comparing the minimum of the chemical exergy plot (Figure 6) against the chemical exergy that would occur if complete combustion occurred (i.e. to produce only CO_2, H_2O, N_2, and excess O_2), the exergy loss due to incomplete combustion is quantified. Using these insights from the crank-angle resolved exergy analysis over a large number of operating conditions, we can understand the relative impact of different loss mechanisms and how they change with varying engine operating conditions. Additionally, by comparing the physical exergy of exhaust gases against the physical exergy of intake gases, we can understand the practicality and design requirements for turbocharging.

3.2 Understanding the Influence of Engine Operating Parameters on Exergy Destruction

The crank-angle resolved exergy analysis is post-processed to generate summary data that shows the relative influence of four specific exergy loss mechanisms: 1) irreversible combustion, 2) heat loss from the in-cylinder gases through the cylinder walls, head and piston, 3) physical exergy lost to the exhaust gases, and 4) chemical exergy that cannot be used because of incomplete combustion.

The impact of these different loss mechanisms on overall exergy efficiency is explored in the three subsections below. Each sub-section explores the impact of different parameters for changing the engine power output, including 1) an intake pressure sweep, 2) an equivalence ratio sweep, and 3) an engine speed sweep.

Within each subsection, two types of plots are presented which show the impact of exergy loss mechanisms on the y-axis. The first set of plots in each section has combustion timing on the x-axis and shows a complete sweep of combustion timings, with CA50 starting slightly before TDC and sweeping through combustion timings until misfire occurs. Different colors are used to identify the different loss mechanisms, while different line styles and symbols identify a sweep through the parameter of interest (intake pressure, equivalence ratio, or engine speed). This first style of plot makes it very easy to identify the relative contribution of each loss mechanism over a wide range of operating conditions.

The second style of plot in each section shows specific parameters of interest on the x-axis (i.e. intake pressure, equivalence ratio, or engine speed). This plot style takes a small subset of the data from the first plot style by only showing data at combustion timings of CA50=365° and 370°. This plot style makes it easier to identify how changes in intake pressure, equivalence ratio, and engine speed influence the different loss mechanisms.

3.2.1 Intake Pressure Sweep

Figure 8 shows the exergy loss mechanisms for a range of intake pressures and for combustion timings from slightly before TDC (360°) to misfire. The figure is generated from crank-angle resolved exergy analysis of 72 different cycle simulations, each representing a different intake pressure and combustion timing, with ϕ=0.40, 1800 RPM and ethanol fueling maintained for all operating points. The results show that over the range of intake pressures and combustion timings explored, irreversible combustion causes between 18.3-20.5% of exergy loss, unused physical exergy in the exhaust causes between 14.8-18.2% of exergy loss, heat loss causes between 4.4-13.3% of exergy loss, and inaccessible chemical exergy from incomplete combustion causes between 4.7-29.1% exergy loss.
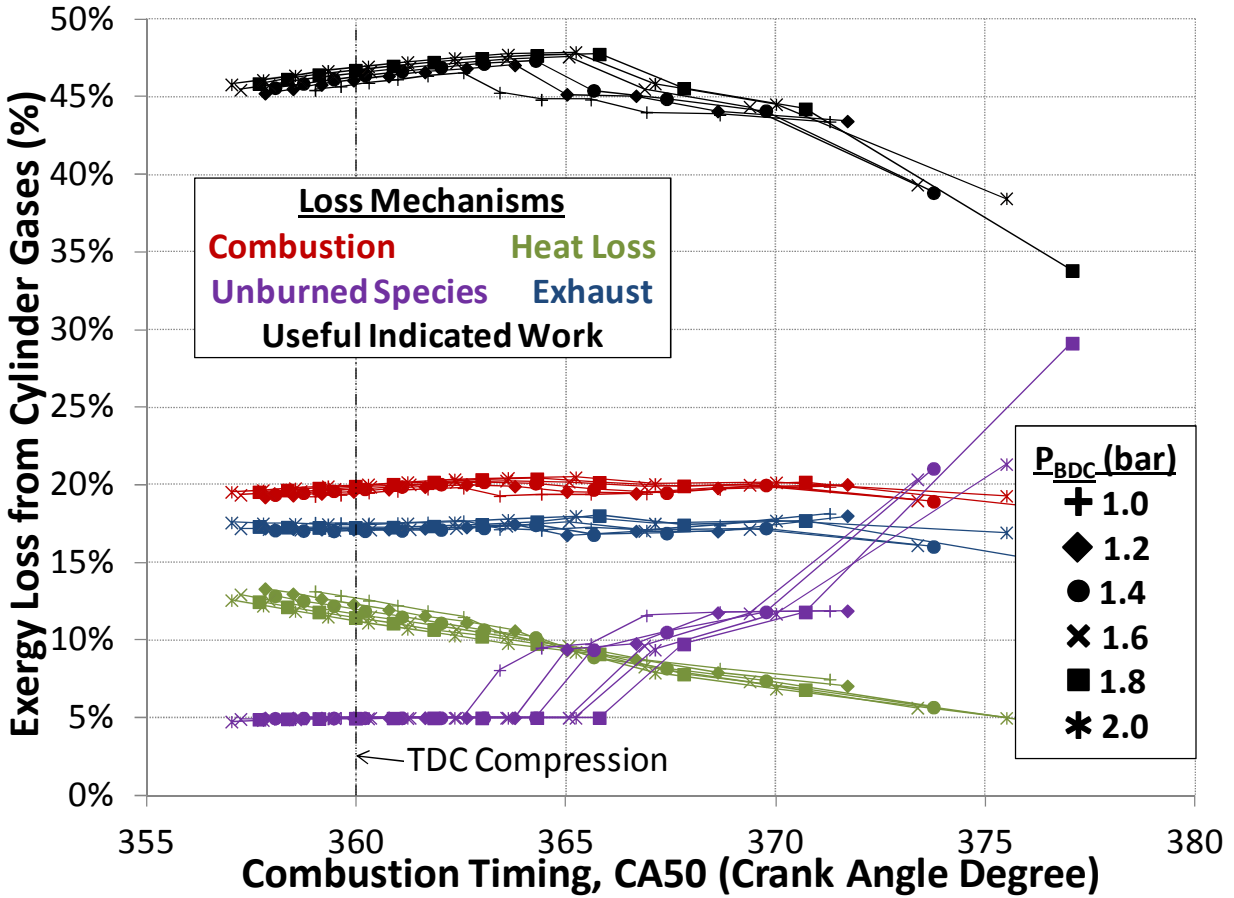
Figure 8 - BDC pressure and combustion timing sweep of exergy loss mechanisms for φ=0.40, 1800 RPM, Ethanol fuel

Figure 8 shows that the mechanisms of irreversible combustion and unused physical exergy in the exhaust are only mildly sensitive to changes in combustion timing, and thus the maximum exergy efficiency point for the different intake pressures (for φ=0.40, 1800 RPM, ethanol fuel) is governed predominantly by the balance between exergy loss from heat losses and exergy loss from incomplete combustion. Consistent with prior knowledge [11,21], exergy losses from heat loss decrease (roughly linearly) with delayed combustion timing, and exergy losses from incomplete combustion increase sharply with delayed combustion timing. It is particularly important to note that the combustion timing delay which acts as the threshold for sharp increases in exergy loss from incomplete combustion is further delayed with increasing intake pressures. The influence of intake pressure upon combustion parameters is seen more clearly in Figure 9, which plots data points for fixed combustion timings (CA50=365° and 370°) along an x-axis of intake pressure.
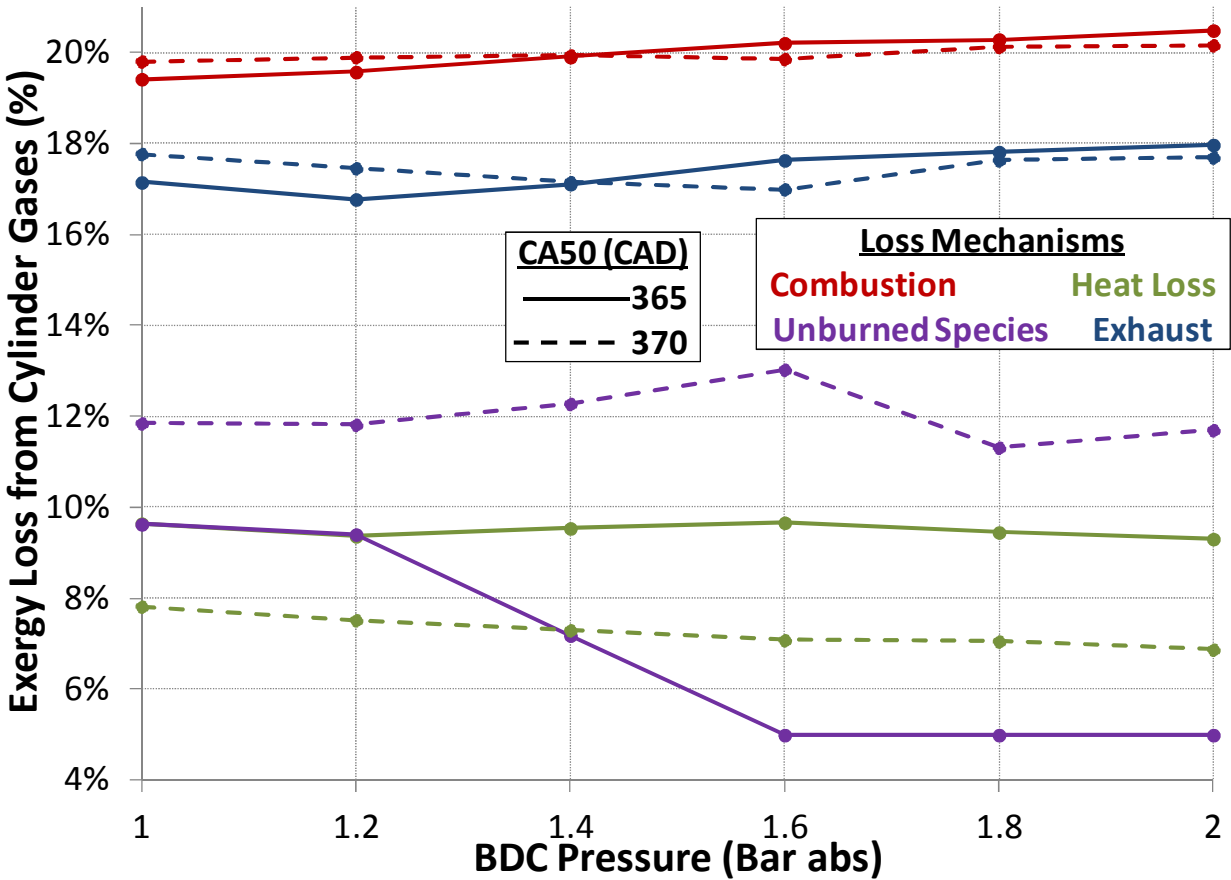
Figure 9 - BDC pressure sweep of exergy loss mechanisms for φ=0.40, 1800 RPM, CA50=365° and 370°, Ethanol fuel

Figure 9 shows only minor changes in exergy loss from irreversible combustion and unused physical exergy in exhaust gases as intake pressures are increased. At a combustion timing of 365°, exergy loss from heat loss is not very sensitive to changes in intake pressure, however, at further delayed combustion timings, 370°, exergy losses from heat loss decrease slightly with increasing intake pressure. Referring back to heat loss contours in Figure 8, it is important to observe that at TDC (360°), exergy loss from heat loss appears more sensitive to intake pressure. From Figure 8 it is apparent that changes in losses from incomplete combustion due to varying intake pressure are only apparent at intermediate combustion timings. Thus in Figure 9, exergy loss from incomplete combustion decreases with increasing intake pressure at CA50=365° while at CA50=370°, the exergy losses from incomplete combustion no longer have a significant intake pressure dependence. In terms of applicability to engine design, Figure 8 shows that as intake pressures are increased, more delayed combustion timing can be used before losses from incomplete combustion increase substantially.

3.2.2 Equivalence Ratio Sweep

In this section, the impacts of changing fuel-air equivalence ratio are explored for two different intake pressures (P_{BDC}=1.0 bar in Figure 10 and Figure 11, then P_{BDC}=1.8 bar in Figure 12 and Figure 13). Figure 10 and Figure 12 show the exergy loss mechanisms for a range of equivalence ratios and for combustion timings from slightly before TDC (360°) to misfire. Each figure is generated from crank-angle resolved exergy analysis of 60 different cycle simulations, each representing a different equivalence ratio and combustion timing, with an engine speed of 1800 RPM and ethanol fueling for all operating points.

The results in Figure 10 show that over the range of equivalence ratios and combustion timings explored (for

P$_{BDC}$=1.0 bar), irreversible combustion causes between 16.4-20.8% of exergy loss, unused physical exergy in the exhaust causes between 13.0-18.7% of exergy loss, heat loss causes between 4.6-13.9% of exergy loss, and inaccessible chemical exergy from incomplete combustion causes between 5.0-36.9% exergy loss.
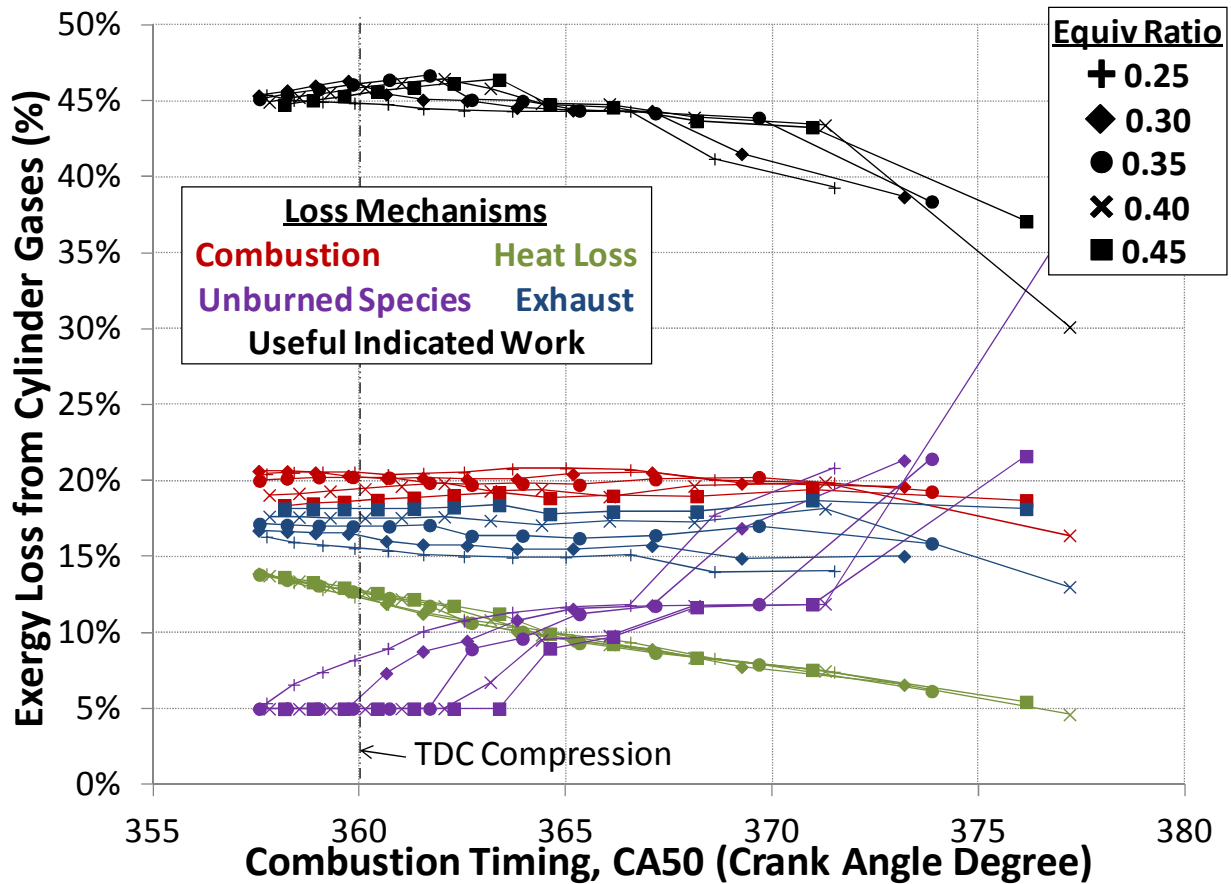

Figure 10 - Equivalence ratio and combustion timing sweep of exergy loss mechanisms for P$_{BDC}$=1.0 bar, 1800 RPM, Ethanol fuel

Figure 10 shows that the mechanisms of irreversible combustion and unused physical exergy in the exhaust are only mildly sensitive to changes in combustion timing (consistent with Figure 8), however there is a greater sensitivity to changes in equivalence ratio (explored further in Figure 11). Also consistent with Figure 8, exergy losses from heat loss decrease with delayed combustion timing. Exergy losses from incomplete combustion increase with delayed combustion timing beyond a certain threshold of sufficiently delayed combustion timing. The threshold for the occurrence of exergy losses from incomplete combustion occurs with further delayed combustion timing as higher equivalence ratios are used. Figure 11 directly shows the equivalence ratio influence on loss mechanisms for two combustion timings, CA50=365° and 370°.
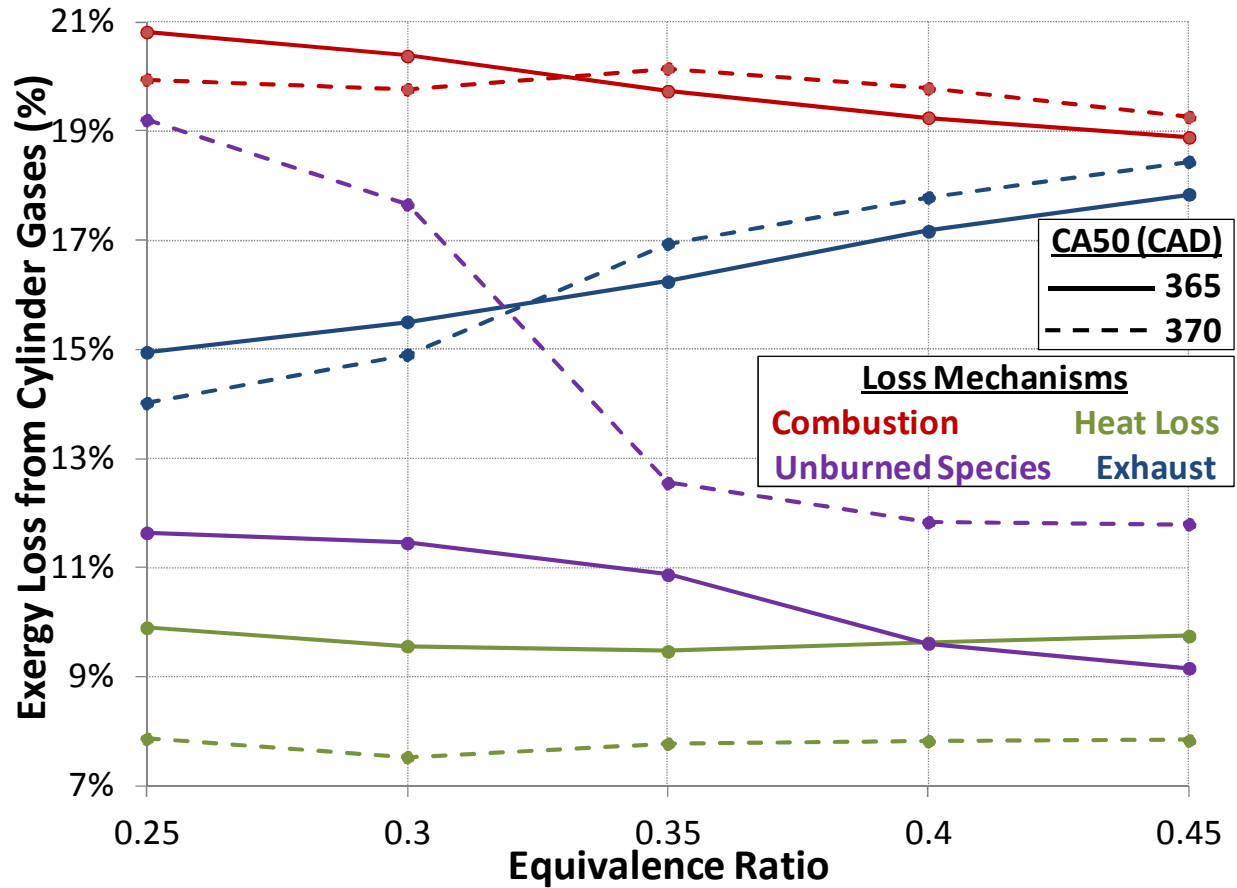
15

**Figure 11 - Equivalence ratio sweep of exergy loss mechanisms
for P$_{BDC}$=1.0 bar abs, 1800 RPM, CA50=365° and 370°, Ethanol fuel**

Figure 11 shows that the contribution of exergy losses from irreversible combustion decreases with increasing equivalence ratio, particularly for earlier combustion timings. This trend is probably the result of increased internal heat exchange to raise the temperature of increased amounts of non-reactive species (i.e. more excess N_2 and O_2) [23]. The contribution of unused physical exergy lost to exhaust gases also increases with higher equivalence ratios, and the amount of this increase is slightly higher for delayed combustion timing. The fraction of exergy losses to heat loss remains relatively insensitive to changes in equivalence ratio. Finally, the contribution of exergy loss from incomplete combustion decreases with increasing equivalence ratios, particularly for further delays in combustion timing.

Figure 12 and Figure 13 show similar plots illustrating the influence of equivalence ratio on loss mechanisms, but for a higher pressure of P$_{BDC}$=1.8 bar abs. The results from Figure 12 show that irreversible combustion causes between 18.3-21.5% of exergy loss, unused physical exergy in the exhaust causes between 13.7-18.7% of exergy loss, exergy losses from heat loss cause between 4.4-12.5% of exergy loss, and inaccessible chemical exergy from incomplete combustion causes between 4.9-29.1% of exergy loss.
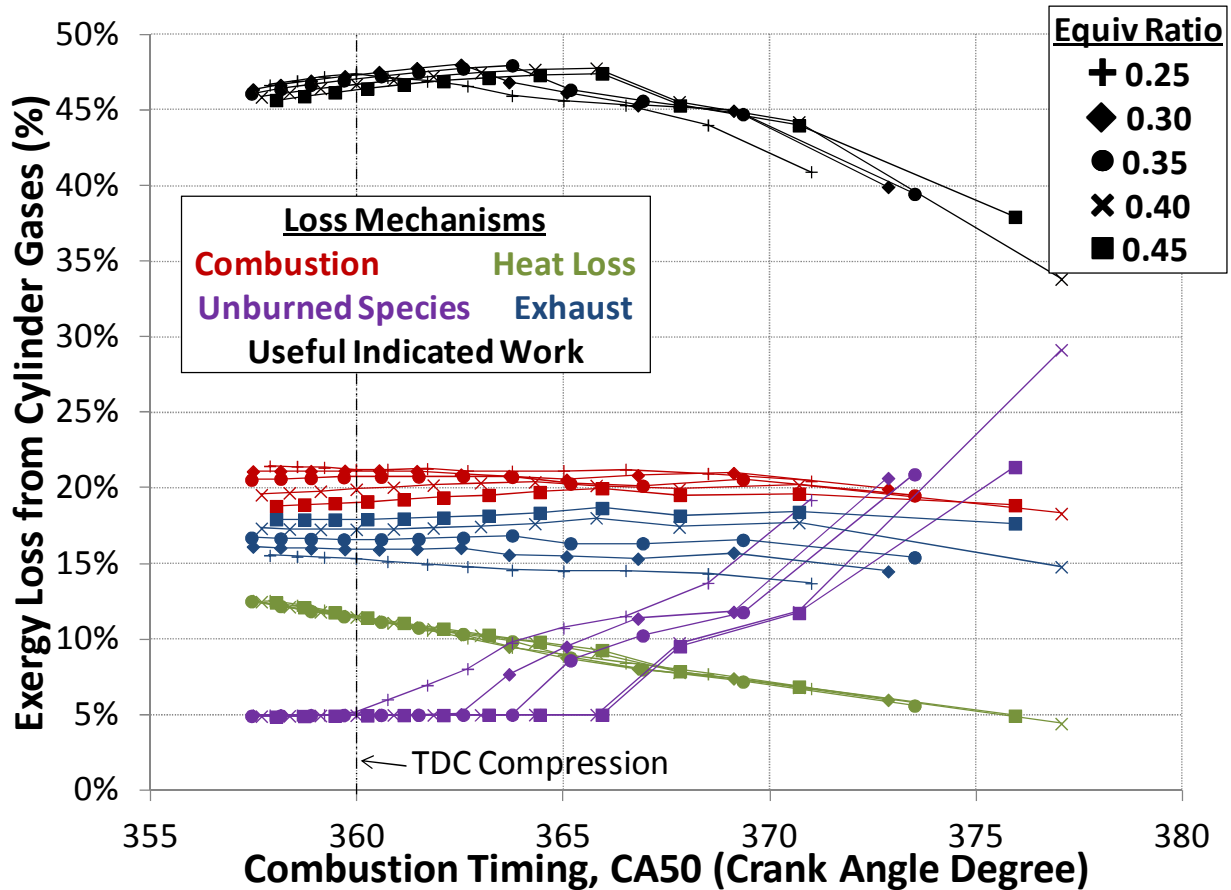
Figure 12 - Equivalence ratio and combustion timing sweep of exergy loss mechanisms for PBDC=1.8 bar, 1800 RPM, Ethanol fuel

Consistent with the Figure 10 (P$_{BDC}$=1.0 bar), Figure 12 (P$_{BDC}$=1.8 bar) shows that irreversible combustion and unused physical exergy in the exhaust are only mildly sensitive to changes in combustion timing, however there is a greater sensitivity to changes in equivalence ratio. For this case too, heat loss decreases with delayed combustion timing. In further agreement with earlier cases, exergy losses from incomplete combustion increase with delayed combustion timing beyond a certain threshold of sufficiently delayed combustion timing. By comparing Figure 10 and Figure 12 it is apparent that higher equivalence ratios and higher intake pressures cause this threshold of increased exergy loss from incomplete combustion to occur with later combustion timings. Figure 13 directly shows the equivalence ratio influence on loss mechanisms for two combustion timings, 365° and 370°, for a pressure of P$_{BDC}$=1.8 bar abs.
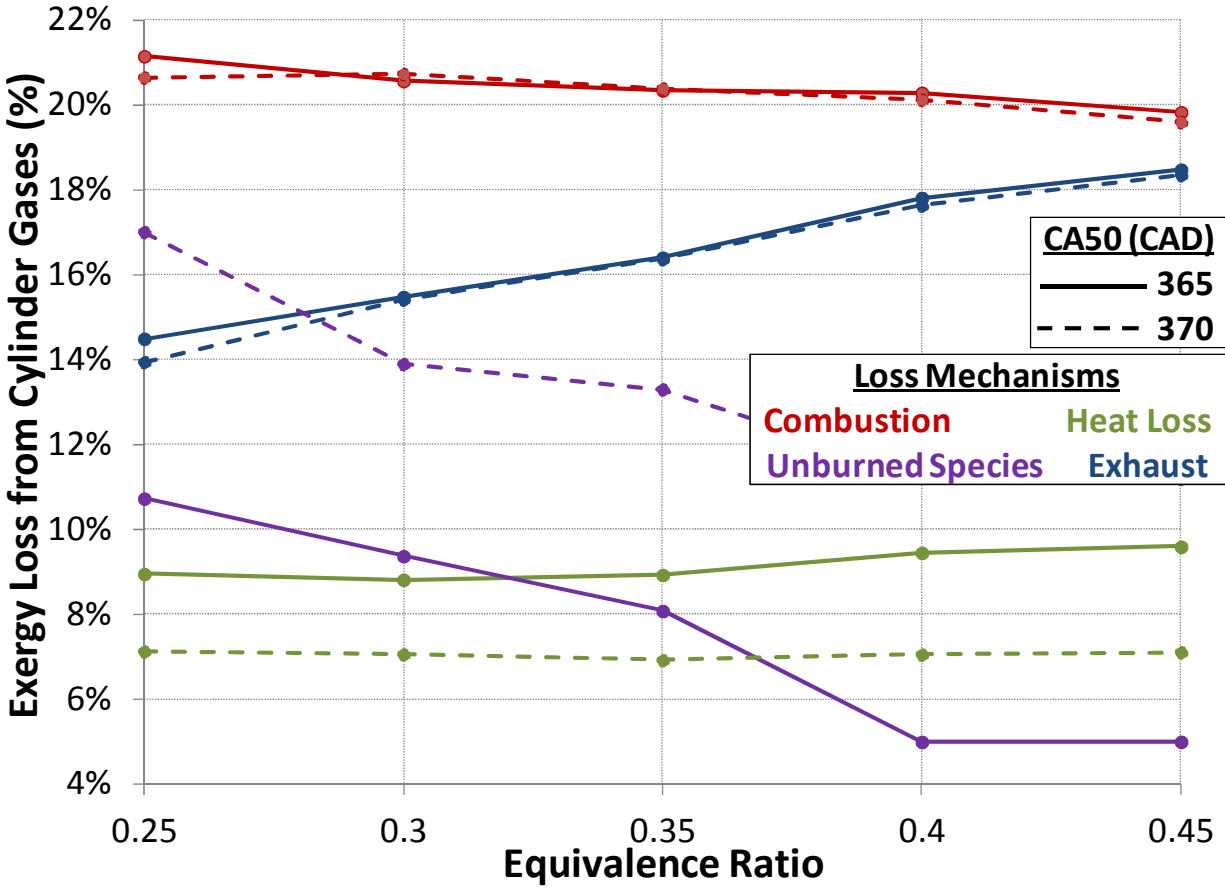
Figure 13 - Equivalence ratio sweep of exergy loss mechanisms for P_{BDC}=1.8 bar abs, 1800 RPM, CA50=365° and 370°, Ethanol fuel

Figure 13 shows that the contribution of exergy loss from irreversible combustion decreases slightly with increasing equivalence ratio, although by comparing Figure 11 (P_{BDC}=1.0 bar) and Figure 13 (P_{BDC}=1.8 bar) it is apparent that the rate of this decrease is lower for higher intake pressure cases. The contribution of unused physical exergy lost to exhaust gases increases with higher equivalence ratios and by comparing the 1.0 and 1.8 bar cases the rate of this increase is larger for the higher intake pressure case. The contribution of exergy loss from heat loss slightly increases with (CA50=365°) or is insensitive to (CA50=370°) increased equivalence ratio. Consistent with Figure 11, exergy losses due to incomplete combustion decrease with higher equivalence ratio.

3.2.3   Engine Speed Sweep

Figure 14 shows the exergy loss mechanisms for a range of engine speeds and for combustion timings from slightly before TDC (360°) to misfire. The figure is generated from 72 different cycle simulations, each representing a different engine speed and combustion timing, with P_{BDC}=1.8 bar, ϕ=0.40 and ethanol fueling maintained for all operating points. Figure 14 shows that over the range of engine speeds and combustion timings explored, irreversible combustion causes 16.7-20.7% of exergy loss, unused physical exergy in the exhaust causes between 12.0-18.3% of exergy loss, heat loss causes between 3.9-17.1% of exergy loss, and inaccessible chemical exergy from incomplete combustion causes between 4.8-37.8% of exergy loss.
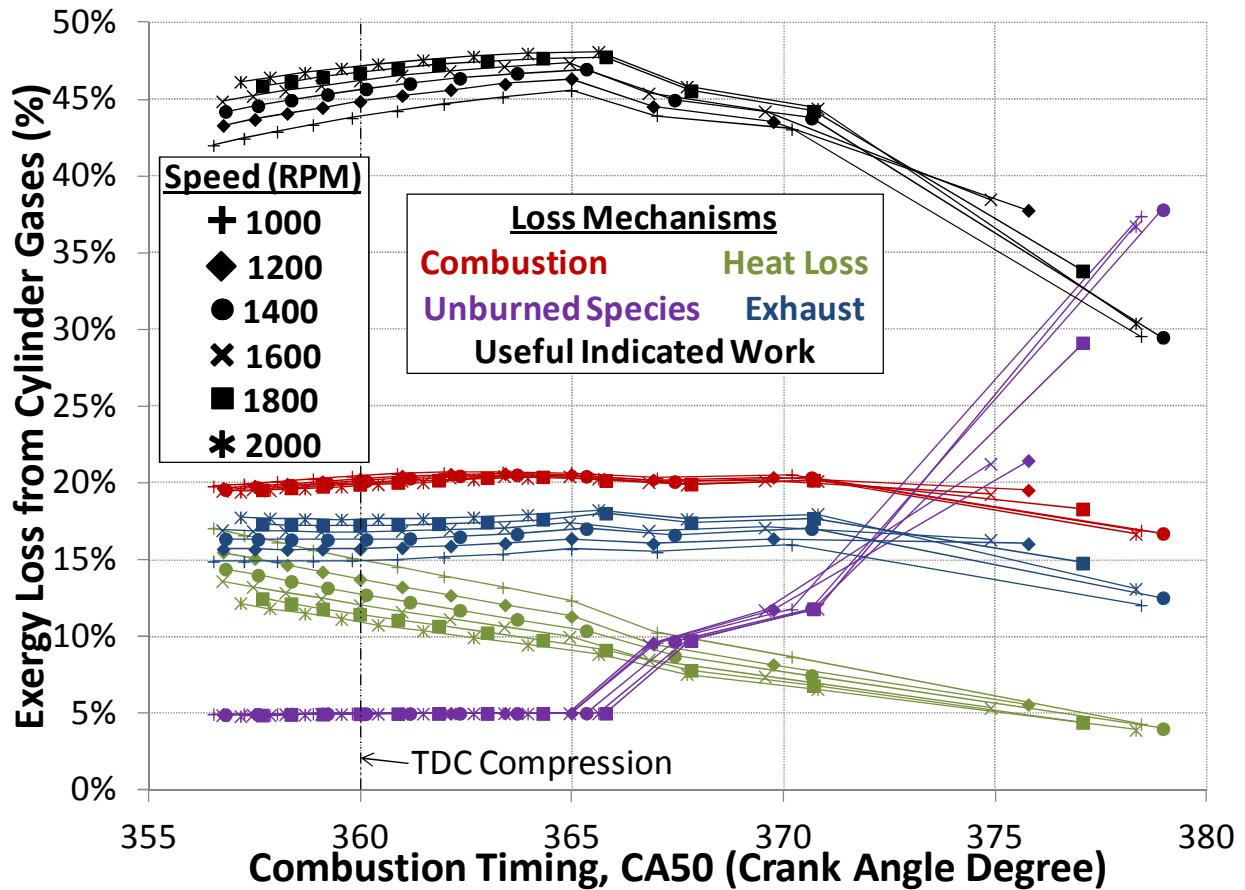
**Figure 14 - Engine speed and combustion timing sweep
of exergy loss mechanisms for P_{BDC}=1.8 bar, ϕ=0.40, Ethanol fuel**

Consistent with earlier figures, Figure 14 shows that the loss mechanisms of irreversible combustion and unused physical exergy to exhaust gases are insensitive to combustion timing, while exergy loss from heat loss decreases with delayed combustion timing. Exergy loss from incomplete combustion increases with delayed combustion timing beyond a threshold of combustion timing delay. Figure 15 shows the engine speed influence on loss mechanisms more clearly by presenting data points for two combustion timings, CA50=365° and 370°.
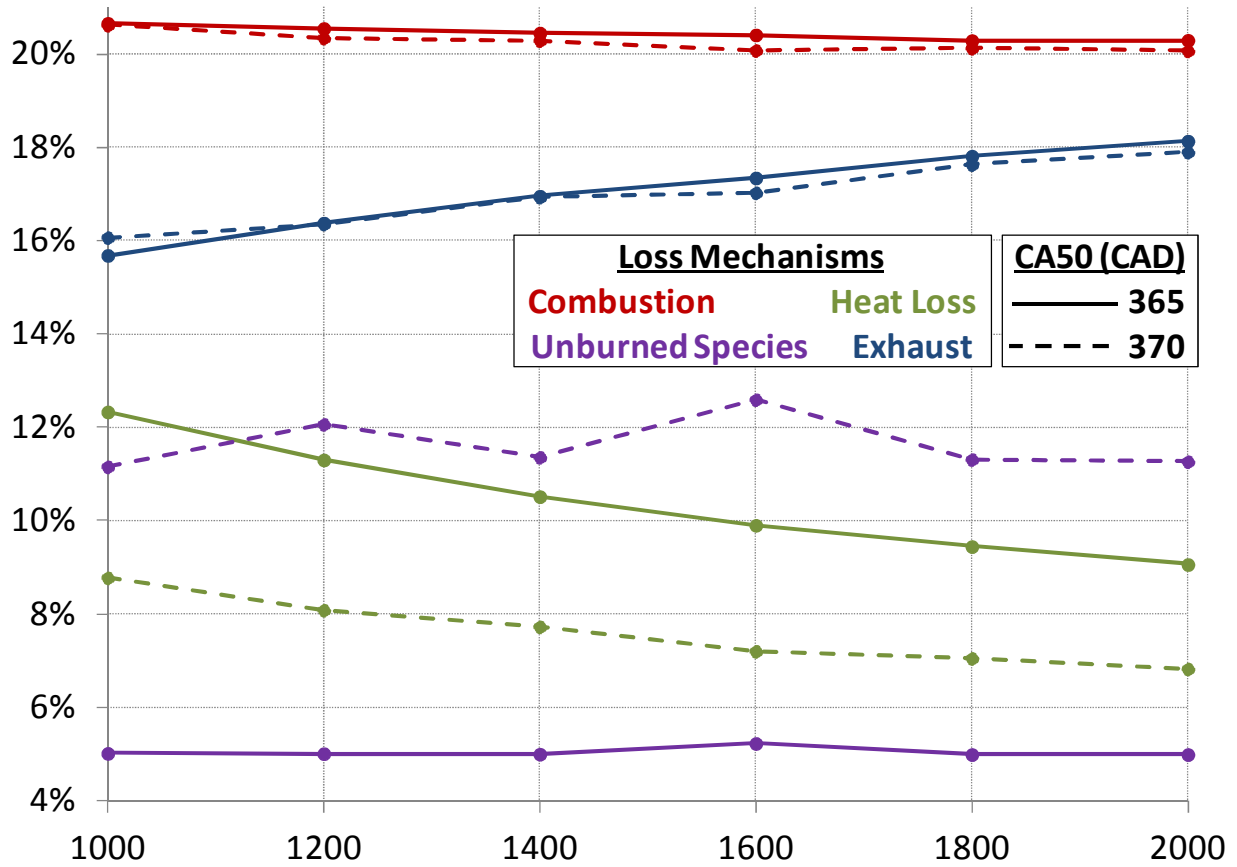
**Figure 15 - Engine speed sweep of exergy loss mechanisms
for P$_{BDC}$=1.8 bar abs, ϕ=0.40, CA50=365° and 370°, Ethanol fuel**

Figure 15 shows that exergy loss from irreversible combustion remains relatively constant across different engine speeds, while unused physical exergy lost in exhaust gases increases with increasing engine speed. Exergy losses from heat loss decrease with increasing engine speed. For CA50=365° and 370°, exergy loss from incomplete combustion is insensitive to changes in engine speed.

4   Using Exergy Analysis for Engine Design

The information provided by exergy analysis can be used during engine research and design processes. Section 3.1 demonstrated the insight that can be gained from crank-angle resolved exergy analysis, and section 3.2 showed how this technique can be used to understand how loss mechanisms change as different engine parameters are varied to influence the power output. This breakdown of exergy loss mechanisms can be used to prioritize research investment decisions by providing insight into the relative importance of each loss mechanism for various operating conditions. By comparing the loss mechanisms for HCCI engines against different engine types, or the loss mechanisms of different HCCI engine designs, structural design decisions can also be made. For ethanol fueled HCCI, the exergy loss from irreversible combustion is difficult to minimize further, and the results show that the relative impact of this loss mechanism remains fairly constant over the entire range of operating conditions explored. The other losses can be absorbed or reduced through techniques like turbocharging, thermal linings or by using smaller crevice zones. In choosing which research and development techniques to use to achieve higher efficiencies, the exergy analysis approach presented in this paper allows the researcher aiming to improve efficiency to understand the theoretical maximum efficiency gain that could be achieved through any research effort. For instance, the results show that more potential exists for trying to recover exergy losses to exhaust gases rather than trying to reduce heat losses. In this process, it is also important to consider engine design constraints (like excessive ringing, in-cylinder pressure limits, etc.). Overlaying constraints will automatically eliminate operating conditions; for example, by overlaying ringing intensity on the exergy loss plots, it will become apparent that early combustion timings are not desirable and thus the research focus will turn to minimizing losses due to incomplete combustion. An immediate research task for the authors is to implement this exergy analysis methodology using a more advanced simulation technique [15] so that constraints like ringing can be considered simultaneously with the loss mechanisms.

Comparing the physical availability of the in-cylinder charge at exhaust valve open and intake valve close can also provide insight for turbocharger design. Figure 16 presents a sample plot which compares the physical availability of intake and exhaust charges for an equivalence ratio sweep (for the same operating point as Figure 12), however it is important to include models of the intake and exhaust processes, and a turbocharger model to provide conclusive information to guide turbocharger design. Implementing detailed exergy analysis on in-cylinder processes, as was done in this paper, should be combined with intake and exhaust processes to quantify and prioritize all of the loss mechanisms in a holistic engine design process.
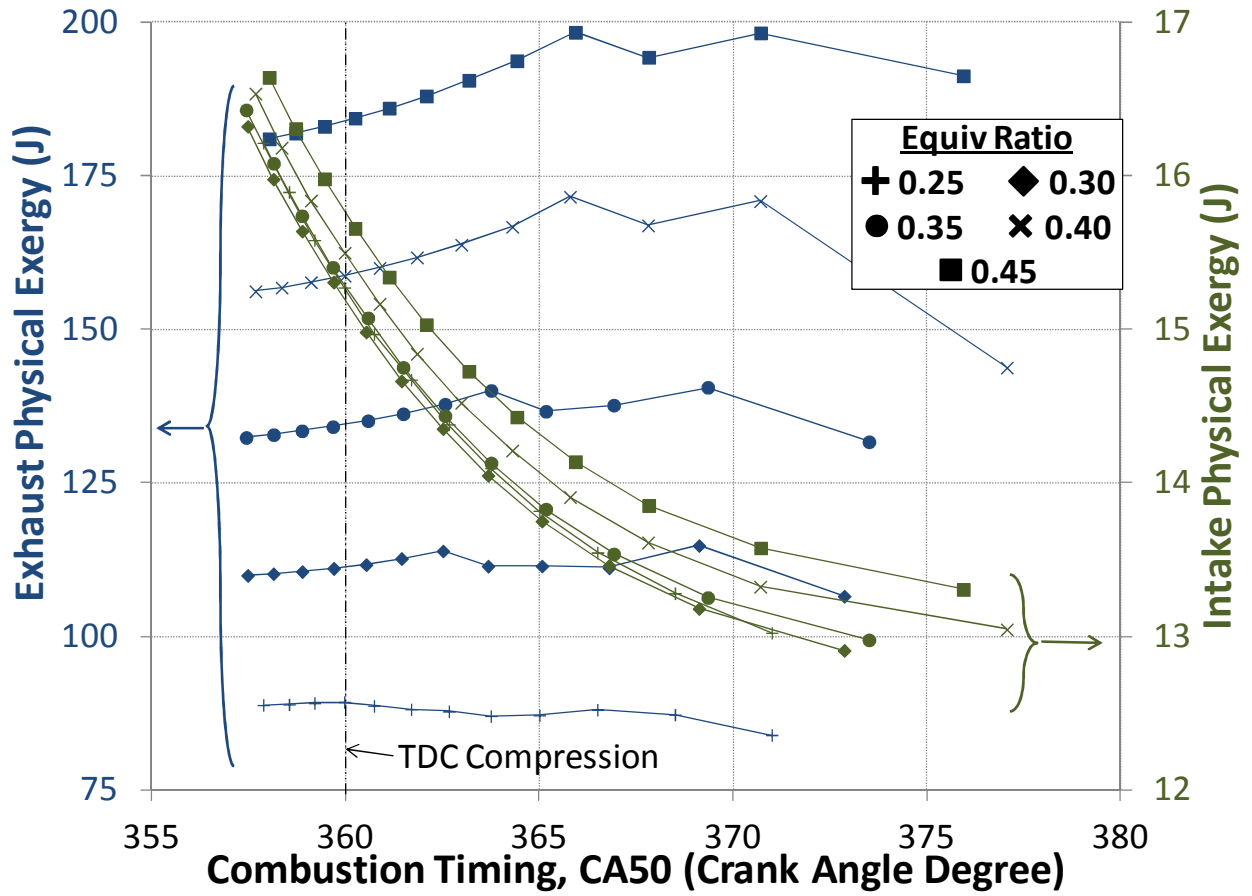
Figure 16 - Comparison of intake and exhaust physical availability to provide insight for turbocharger design for P_{BDC}=1.8 bar, 1800 RPM, Ethanol fuel

5   Summary and Conclusions

This research provides an understanding of the relative importance of each exergy loss mechanism for an ethanol-fueled HCCI engine. Four loss mechanisms were studied, including, 1) exergy loss from irreversible combustion, 2) physical exergy lost to the exhaust gases, 3) exergy loss to heat loss, and 4) inaccessible chemical exergy due to incomplete combustion. The trends in each loss mechanism were studied over different intake pressures, equivalence ratios, engine speeds and combustion timings. The following trends and results are identified for ethanol-fueled HCCI engines:

1. The fraction of exergy loss from irreversible combustion constitutes 16.4-21.5% of overall exergy loss. It does not change significantly with different intake pressures, equivalence ratios, engine speeds, and combustion timings.

2. The fraction of exergy loss from physical exergy lost to exhaust gases constitutes 12.0-18.7% of overall exergy loss. It is not sensitive to changes in intake pressure, or combustion timing, however it increases with increasing equivalence ratio and engine speed.

3. The fraction of exergy loss from heat loss constitutes 3.9-17.1% of overall exergy loss. It is relatively insensitive to changes intake pressure, however, for delayed combustion timing, it decreases slightly with increasing intake pressure. There is little sensitivity to changes in equivalence ratio. It decreases with increasing engine speed and delayed combustion timing.

4. The fraction of exergy loss from incomplete combustion constitutes 4.7-37.8% of overall exergy loss. It remains relatively constant at early combustion timings, but rises sharply as combustion timing is delayed beyond a certain threshold. The combustion timing where this threshold occurs is earlier with lower intake pressures and lower equivalence ratios. The threshold is relatively insensitive to changes in engine speed.

Crank-angle resolved exergy analysis provides useful insights to guide the research and design processes. By quantifying the relative contributions and trends in the various loss mechanisms, research targeting efficiency improvements (for example, the use of thermal barriers on the cylinder boundaries, exhaust exergy recovery, or better choice of operating parameters) can be prioritized more effectively. Furthermore, by overlaying engine design constraints with these loss mechanisms, engine mapping processes during the design process can be performed more effectively.

6 Acknowledgments

7 References

[1] Caton, J.A., 2000, "On the Destruction of Availability (Exergy) due to Combustion Processes – with Specific Application to Internal-Combustion Engines," Energy, 25(11), pp. 1097-1117, doi: 10.1016/S0360-5442(00)00034-7.

[2] Caton, J.A., 2012, "Exergy Destruction During the Combustion Process as Functions of Operating and Design Parameters for a Spark-Ignition Engine," Int. J. Energy Res., 36(3), pp. 368-384, doi: 10.1002/er.1807.

[3] Edwards, K.D., Wagner, R.M., Briggs, T.E., and Theiss, T.J., 2011, "Defining Engine Efficiency Limits", 17th DEER Conference, Detroit, MI.

[4] Khaliq, A., and Trivedi, S.K., 2012, "Second Law Assessment of a Wet Ethanol Fuelled HCCI Engine Combined With Organic Rankine Cycle," ASME J. Energy Resour. Technol., 143(2), doi: 10.1115/1.4005698.

[5] Khaliq, A., Trivedi, S.K., and Dincer, I., 2012, "Investigation of a wet ethanol operated HCCI engine based on first and second law analyses," Appl. Thermal Eng., 31(10), pp. 1621-1629, doi: 10.1016/j.applthermaleng.2011.02.001.

[6] Amjad, A.K., Saray, R.K., Mahmoudi, S.M.S., and Rahimi, A., 2011, "Availability Analysis of n-heptane and Natural Gas blends Combustion in HCCI Engines," Energy, 36(12), pp. 6900-6909, doi: 10.1016/j.energy.2011.09.046.

[7] Aceves, S.M., Flowers, D.L., Martinez-Frias, J., Smith, J.R., Westbrook, C., Pitz, W., Dibble, R., Wright, J.F., Akinyemi, W.C., and Hessel, R.P., 2001, "A Sequential Fluid-Mechanic Chemical-Kinetic Model of Propane HCCI Combustion," SAE Technical Paper 2001-01-1027, doi: 10.4271/2001-01-1027.

[8] Woschni, G., 1967, "A Universally Applicable Equation for the Instantaneous Heat Transfer Coefficient in the Internal Combustion Engine," SAE Technical Paper 670931, doi: 10.4271/670931.

[9] Heywood, J.B., 1988, Internal Combustion Engines Fundamentals, McGraw-Hill, New York, pp. 145.

[10] Marinov, N.M., 1999, "A Detailed Chemical Kinetic Model for High Temperature Ethanol Oxidation," Int. J. Chem. Kinet., 31, pp. 183-220.

[11] Saxena, S., Chen, J-Y, and Dibble, R., 2011, "Maximizing Power Output in an Automotive Scale Multi-Cylinder Homogeneous Charge Compression Ignition (HCCI) Engine," SAE Technical Paper 2011-01-0907, doi: 10.4271/2011-01-0907.

[12] Saxena, S., 2011, "Maximizing Power Output in Homogeneous Charge Compression Engines and Enabling Effective Control of Combustion Timing," Ph.D Dissertation.

[13] Saxena, S., Schneider, S., Aceves, S., and Dibble, R., 2012, "Wet Ethanol in HCCI Engines with Exhaust Heat Recovery to Improve the Energy Balance of Ethanol Fuels," Applied Energy, doi: 10.1016/j.apenergy.2012.04.007.

[14] Bedoya, I.D., Saxena, S., Cadavid, F.J., and Dibble, R.W., 2012, "Exploring Strategies for Reducing High Intake Temperature Requirements and Allowing Optimal Operational Conditions in a Biogas Fueled HCCI Engine for Power Generation," ASME Journal of Eng. for Gas Turbines and Power, GTP-11-1387, doi: 10.1115/1.4006075

[15] Bedoya, I.D., Cadavid, F., Saxena, S., Dibble, R., Aceves, S., and Flowers, D., 2012, "A Sequential Chemical Kinetics-CFD-Chemical Kinetics Methodology to Predict HCCI Combustion and Main

Emissions," SAE Technical Paper 2012-01-1119, doi: 10.4271/2012-01-1119.

[16] Flowers, D.L., Aceves, S.M., Martinez-Frias, J., and Dibble, R.W., 2002, "Prediction of carbon monoxide and hydrocarbon emissions in iso-octane HCCI engine combustion using multizone simulations," Proc. Combustion Institute, 29(1):687-694, doi: 10.1016/S1540-7489(02)80088-8.

[17] Flowers, D.L., Aceves, S.M., Martinez-Frias, J., Hessel, R., and Dibble, R.W., 2003, "Effect of Mixing on Hydrocarbon and Carbon Monoxide Emissions Prediction for Isooctane HCCI Engine Combustion Using a Multi-zone Detailed Chemical Kinetics Solver," SAE Paper 2003-01-1821, doi: 10.4271/2003-01-1821.

[18] Cheng, W.K., Summers, T., and Collings, N., 1998, "The fast-response flame ionization detector," Prog. Energy Combust. Sci., 24(2):89-124, doi: 10.1016/S0360-1285(97)00025-7.

[19] Bejan, A., 2006, Advanced Engineering Thermodynamics, John Wiley and Sons, Hoboken, NJ.

[20] Szargut, J., Morris, D.R., and Steward, F.R., 1988, Exergy Analysis of Thermal, Chemical, and Metallurgical Processes, Hemisphere Publishing, New York.

[21] Sjöberg, M., and Dec, J.E., 2010, "Ethanol Autoignition Characteristics and HCCI Performance for Wide Ranges of Engine Speed, Load and Boost", SAE Technical Paper 2010-01-0338, doi: 10.4271/2010-01-0338.

[22] Dec. J.E., Yang, Y., and Dronniou, N., 2012, "Improving Efficiency and Using E10 for Higher Loads in Boosted HCCI Engines," SAE Technical Paper 2012-01-1107, doi: 10.4271/2012-01-1107.

[23] Dunbar, W.R., and Lior, N., 1994, "Sources of Combustion Irreversibility," Combustion Science and Technology, 103(1-6), pp. 41-61, doi: 10.1080/00102209408907687

8 Appendix: Impact of Number of Zones in Chemical Kinetics Engine Model

To understand the impact of the number of zones used in the multi-zone chemical kinetic model, a parametric study of the number of zones is presented here. For all 252 operating points simulated as part of this research effort, 10 zones were used. A single operating point is chosen to study the impact of number of zones, with P_{BDC}=1.8 bar, T_{BDC}=413.82 K, CA50≈367.8 CAD, ϕ=0.40. Exergy results are compared for 10, 20 and 40 zones. For the 10-zone model, the mass fraction and external heat transfer area fraction are set as follows:

Zone #	Zone mass fraction	External heat transfer area fraction
1	2.0	0.05
2	1.0	0.05
3	1.0	0.05
4	1.0	0.1
5	2.0	0.1
6	5.0	0.15
7	10.0	0.15
8	18.0	0.15
9	25.0	0.1
10	35.0	0.1

Table 4 - Mass fraction and heat transfer fraction used for 10-zone model

The zone mass fraction and external heat transfer area fraction for the 20 and 40 zone models are determined by splitting each zone in the 10 zone model into two, or four separate zones. Figure 17 through Figure 19 show the in-cylinder pressure, in-cylinder temperature and the relative contribution from each exergy loss mechanism for 10, 20 and 40 simulated zones. The results suggest that the number of simulated zones does not influence the exergy analysis results, thus 10 zones is used throughout the paper to minimize computing time for the 252 operating points.
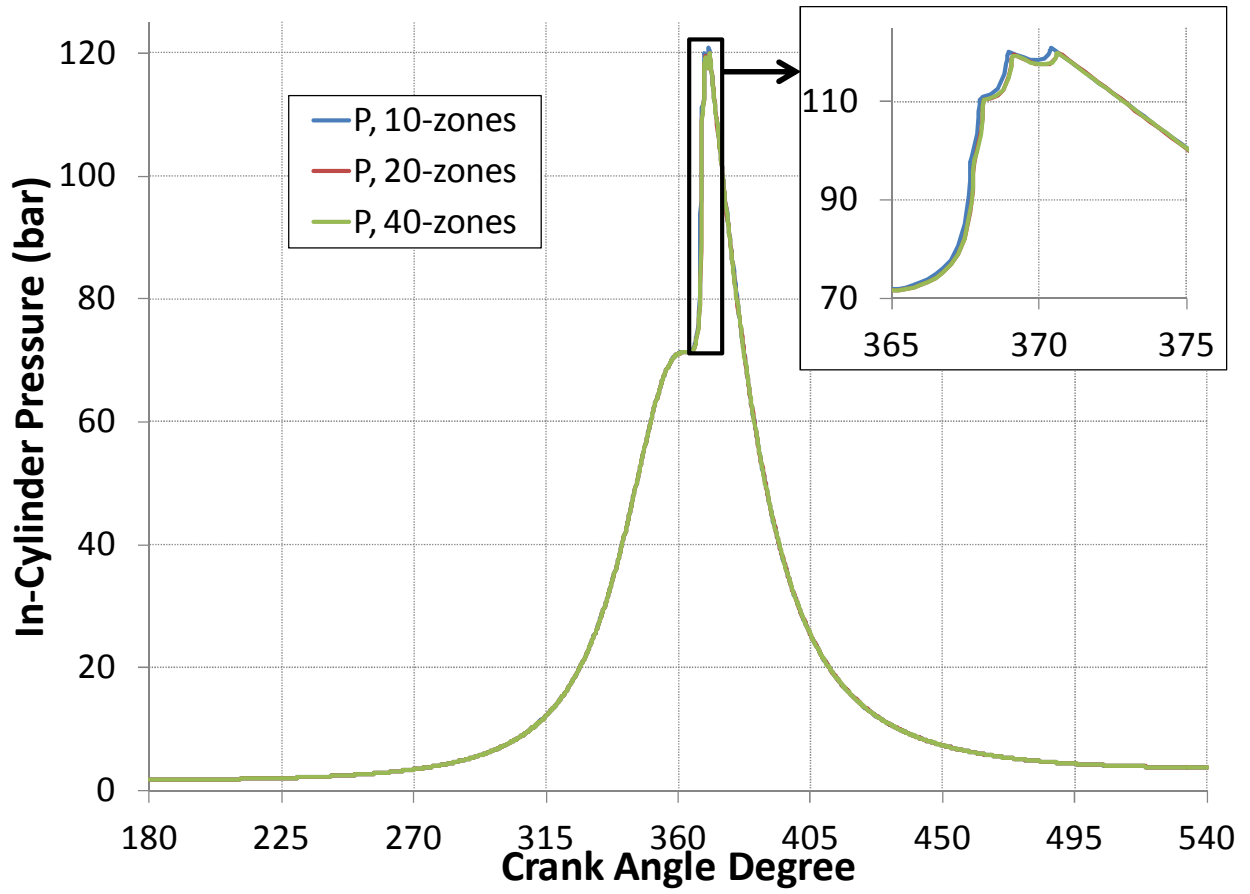
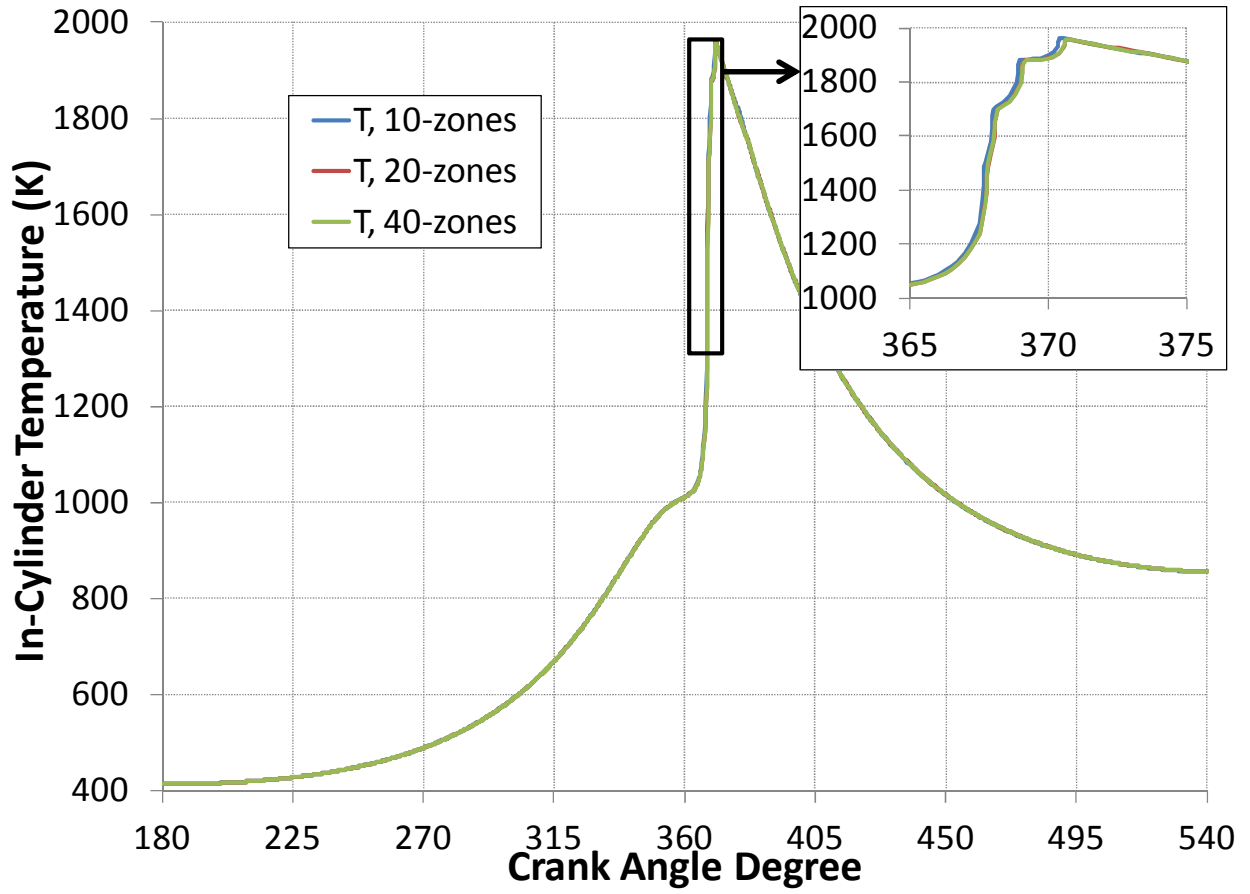Figure 17 - In-cylinder pressure for 10, 20 and 40 zones

Figure 18 - In-cylinder temperature for 10, 20 and 40 zones
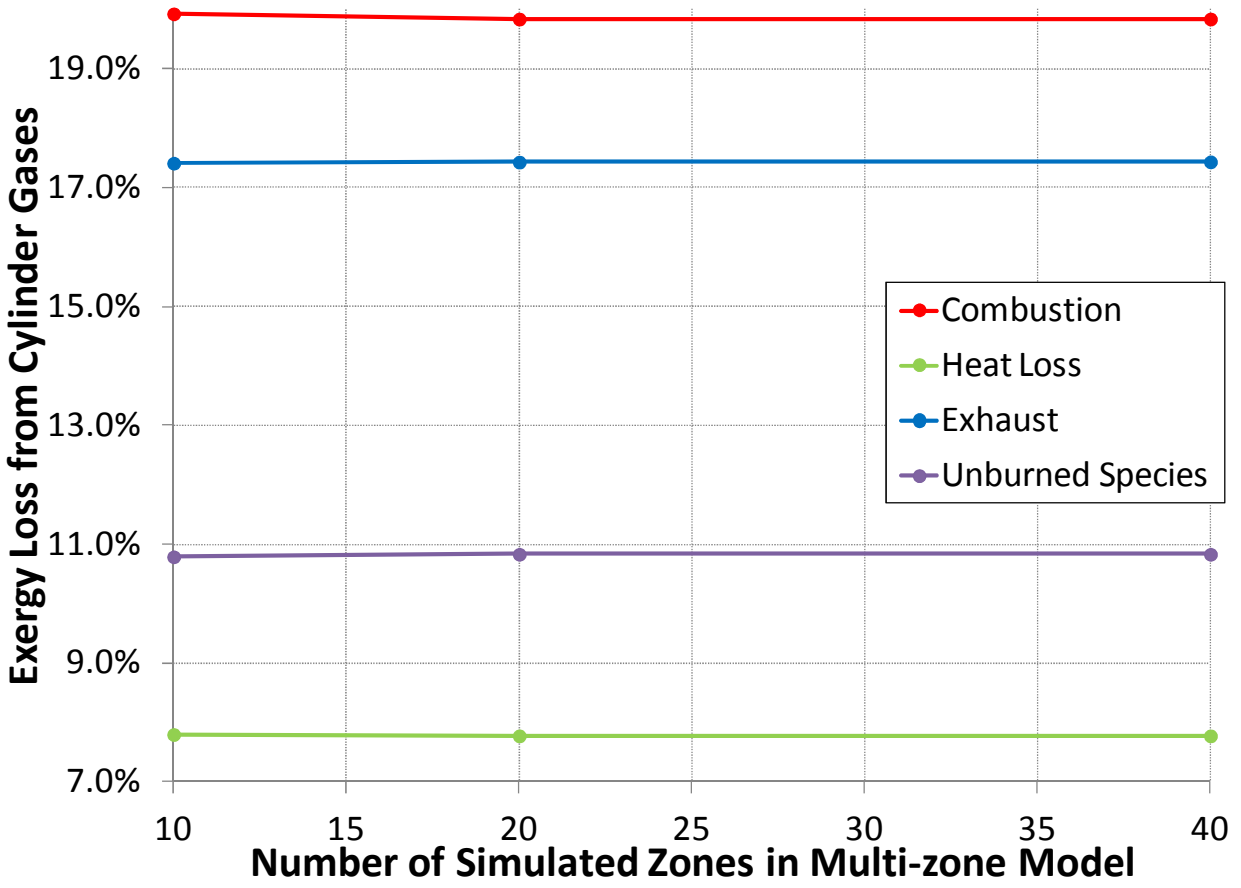
Figure 19 - Contribution of each exergy loss mechanism for 10, 20 and 40 zones